Original Article

Expression of tiRNA and tRF in *APP/PS1* transgenic mice and the change of related proteins expression

Honglin Lu[1], Lin Liu[1], Shu Han[2], Binbin Wang[1], Jin Qin[1], Kailin Bu[1], Yingzhen Zhang[1], Zhongzhong Li[1], Lina Ma[1], Jing Tian[1], Kun Zhang[1], Tong Li[1], Huixian Cui[3], Xiaoyun Liu[1]

[1]Department of Neurology, The Second Hospital of Hebei Medical University, Shijiazhuang, China; [2]Department of Electrocardiogram, The Second Hospital of Hebei Medical University, Shijiazhuang, China; [3]Department of Anatomy, Hebei Medical University, Shijiazhuang, China

Contributions: (I) Conception and design: X Liu; (II) Administrative support: X Liu, H Cui; (III) Provision of study materials or patients: X Liu, H Cui; (IV) Collection and assembly of data: H Lu, L Liu, S Han; (V) Data analysis and interpretation: H Lu, L Liu, S Han, B Wang, J Qin, K Bu, Y Zhang; (VI) Manuscript writing: All authors; (VII) Final approval of manuscript: All authors.

Correspondence to: Xiaoyun Liu. Department of Neurology, The Second Hospital of Hebei Medical University, 215 Heping West Road, Shijiazhuang 050000, China. Email: audrey-l@163.com; Huixian Cui. Department of Anatomy, Hebei Medical University, Shijiazhuang, China. Email: cuihxf@126.com.

Background: Transcriptomics, such as that of non-coding RNA (ncRNA), which include microRNA (miRNA), circular RNA, and the transfer RNA (tRNA)-derived fragments (tiRNA and tRF) in Alzheimer's disease (AD) have attracted much attention recently. The tiRNA and tRFs are produced when the tRNA splits at specific sites. The expression change and related function of tiRNA and tRFs in AD has not been fully investigated.

Methods: In our study, *APP/PS1* transgenic mice (AD mice model) and healthy control mice were used to discover the differentially expressed tiRNA and tRFs with high-throughput sequencing. Among the differentially expressed tiRNA and tRFs, we chose two tRFs (tRF-Thr-CGT-003 and tRF-Leu-CAA-004) and predicted the target messenger RNAs (mRNAs) with miRanda and Target Scan. The target mRNAs of tRF-related function and pathways were analyzed, then we performed quantitative reverse transcription polymerase chain reaction (RT-qPCR) and western blot to validate the related target mRNAs and pathways.

Results: A total of 27 significantly different tiRNA and tRFs were detected between wild type (WT) and *APP/PS1* groups, including 14 up-regulated and 13 down-regulated. Through analyzing the target mRNAs of all differentially expressed tiRNA and tRFs with GO enrichment, we found the target mRNAs could take part in the learning and memory biological process, synapse organization, cognition biological process, synaptic transmission, amyloid-β (Aβ) metabolic process, and so on. We then chose three differentially expressed tRFs for further qPCR validation and passed two tRFs: tRF-Thr-CGT-003 and tRF-Leu-CAA-004, that were found to regulate the calcium regulation-related proteins (the voltage-gated calcium channel γ2 subunit and the RYR1 endoplasmic reticulum calcium released protein) and the retinol metabolism-related proteins (retinoic acid metabolic enzymes *CYP2S1*, *CYP2C68*, *CYP2S1*).

Conclusions: The *APP* expression and presenilin mutation in *APP/PS1* mice could cause tiRNA and tRFs expression change. Among the differentially expressed tiRNA and tRFs, we found some tRFs took part in the voltage-gated calcium channel γ2 subunit expression and regulation, influencing the neuron calcium homeostasis. Moreover, we also found the tRFs may participate in the regulation of retinol metabolism. Our findings suggest that the dysregulated tiRNA and tRFs may be beneficially exploited as potential diagnostic biomarkers and/or therapeutic targets of AD.

Keywords: *APP/PS1* transgenic mice; Alzheimer's disease (AD); tiRNA and tRFs; calcium dysregulation; retinol metabolism

Submitted Jul 23, 2021. Accepted for publication Sep 09, 2021.
doi: 10.21037/atm-21-4318
View this article at: https://dx.doi.org/10.21037/atm-21-4318

Introduction

There were more than 40 million people with dementia worldwide in 2020, and the majority had been diagnosed with Alzheimer's disease (AD). The countries with the largest number of affected individuals are China and the developing western Pacific countries (1). The two core pathological hallmarks of AD are amyloid plaques and neurofibrillary tangles (1-3). The amyloid cascade of AD pathogenesis has been widely explored by researchers, which could induce some biochemical and morphological changes present in AD, including calcium dysregulation, altered cholesterol and phospholipid metabolism, altered mitochondrial dynamics, and impaired bioenergetic function, vascular aging, and so on (3-9). Recently, some researchers have gradually focused their attention on transcriptomics, such as that of non-coding RNA (ncRNA).

With the development of revolutionary deep sequencing technologies, some small ncRNAs (sncRNAs), such as small interfering RNA (siRNA), microRNA (miRNA), and piwi-interacting RNAs (piRNAs) have been shown to regulate diseases such as AD, cancer, and some others (10-13). The miRNAs and piRNAs could regulate some pathological processes of AD, such as regulation of secretases, APP and Tau expression (12), and could affect cognitive evolution (13). In recent years, another sncRNA was discovered and slowly gained recognition, that is transfer RNA (tRNA)-derived fragments (tiRNA and tRFs) which are the fragments cleaved at specific sites of tRNA. These tiRNA and tRFs are not products of random tRNA cleavage or degradation because their ends are precisely defined by RNA cleavage sequence determinants (14). The tiRNA and tRFs could regulate many biological process such as control protein translation as the way of miRNA (15), regulate gene expression (16-18), regulate cellular stress reaction (19,20), and be involved in the regulation of cancers (21,22), virus infection (23,24), metabolic disease (25,26), neurodegenerative diseases, and so on. Pontocerebellar hypoplasia (PCH) with a *CLP1* mutation could result in the abnormal spitting of pre-tRNA which further results in abnormal tiRNA and tRF expression. Angiogenin (ANG, a ribonuclease that cleaves tRNAs) mutation in amyotrophic lateral sclerosis (ALS) could also affect the splitting of tRNA, which were also detected in Parkinson's disease (PD). Recently, it was reported that tRF and tiRNA could increase the expression of Camk2n1 in SAMP8 which could affect the combination of CaMKII and NMDAR, and further suppress the long-term potentiation (LTP), promoting the progression of AD and PD (27). By reanalyzing previous sncRNA raw data from AD patients, Wu *et al.* discovered that there were different tiRNA and tRF expression profiles at different stages of AD. Decreased NSun2 expression could reduce methylation modification, and at the same time ANG expression increased, the tRNA splitting increased and the expression of tiRNA and tRF changed in AD (28).

Based on the length and cleavage sites, tiRNA and tRFs include two main types: one is tiRNA, which is cleaved at the anticodon loop of mature tRNAs with 28–36 nts: tiRNA-5 and tiRNA-3; the other is tRF, which is cleaved at the D-loop and TψC loop of mature tRNA or pre-tRNA with 14–30 nts: tRF-5, tRF-3, tRF-1, tRF-2 (29,30). So far, researchers have discovered that tiRNA and tRFs could participate in many diseases, such as cancers, viral infection, metabolic diseases, neurological diseases (PCH and ALS), epigenetic regulation, moyamoya disease, and ischemic diseases (18,30-32). However, the tiRNA and tRF expression changes in *APP/PS1* mice are poorly understood, so we investigated the regulation of tiRNA and tRFs in an AD model of 11.5–12-month-old *APP/PS1* mice. In our study, we mainly investigated the different expression of tiRNA and tRFs between *APP/PS1* and WT mice, and explored the possible functions that tiRNA and tRF may regulate. We present the following article in accordance with the ARRIVE reporting checklist (available at https://dx.doi.org/10.21037/atm-21-4318).

Methods

Animals and experimental groups

Male wild type (WT) and *APP/PS1* (*APPswe*, *PSEN1dE9* from Jackson Laboratory, Sacramento, CA, USA) mice (11.5–12-month-old, 20–25 g/each mouse) with a genetic background of C57BL/6J were used. The mice were reared with strict specific-pathogen-free (SPF) conditions (room temperature at 25 ℃ and 12 h light-dark cycle), and had free access to standard rodent water and food. Experiments were performed under a project license (No.: 2021-AE026) granted by the Institutional Animal Care Committee of Hebei Medical University, in compliance with AAALAC and the IACUC guidelines for the care and use of animals.

Morris water maze (MWM)

A MWM was used to evaluate the hippocampal-dependent spatial memory (33) (6 mice/each group). The test was

performed in a cylindrical pool (120×38 cm) filled with opaque nontoxic water with a platform (14×6 cm, 1 cm under the water level) located in 1 quadrant, the water temperature was controlled at 24±2 ℃. Extra-maze visual cues were posted around the tank. An overhead camera and SMART software (v3.0, Panlab Tech., Spain) were used to track the mice movements. During the acquisition trial, the mice endured 4 tests (60 s each) each day to find the hidden platform for 5 consecutive days. If the platform was not found within the prescribed time, the mice would be guided to the platform and detained there for 10 s. The sixth day was the probe trial, at which time the platform was removed and the movement trajectory was tracked (60 s for each mouse). During the experiment, the assessor was not visible to the mice while they were swimming.

Immunohistochemistry (IHC)

The WT mice and *APP/PS1* mice (5 mice/each group) were all anesthetized with chloral hydrate and perfused transcardially with ice-cold 4% paraformaldehyde (PFA) in 1× phosphate-buffered saline (PBS, pH 7.3), Then exposed the brains and postfixed with 4% PFA overnight, transferring to 30% sucrose in 1× PBS. Then, the brains were embedded with Optimal Cutting Temperature (O.C.T., Sakura Finetek, Torrance, CA, USA) and stored at –80 ℃. Then, the hippocampal area was sectioned into 30 μm thick coronal sections and stored at –20 ℃ before being processed using IHC. Sections were first washed in 0.01 M PBS 3 times, for 10 min/each time. The sections were punched with 1% Triton X-100 for 30 min and blocked with 0.3% Triton X-100 in PBS, 5% normal goat serum and 1% fetal bovine serum for 1 h at room temperature, following incubation with mice anti-amyloid-β_{42} primary antibody (anti-Aβ_{42}) (1:75; Santa Cruz, Dallas, TX, USA) overnight at 4 ℃. Sections were then washed 3 times, 10 min/each time with 0.01 M PBS before and after incubation with secondary antibody (AlexaFluor-488 anti-mice, 1:500, Thermo Scientific, Waltham, MA, USA) for 2 h at room temperature. The sections were mounted on glass slides, then cover-slipped with DAPI (Boster Biological Engineering Company, Pleasanton, CA, USA) and examined under a Zeiss LSM 510 confocal laser scanning microscopy system (Zeiss, Oberkochen, Germany). The specificity of the Aβ primary antibody was confirmed by incubation of sections with only the secondary antibodies. No immunoreactivity was observed under these conditions.

tiRNA and tRF sample preparation

The mice were divided into two groups: WT and APP (*APP/PS1*) group. After the MWM, the mice were anesthetized with chloral hydrate and immersed with alcohol, dislocated, and the hippocampus was dissected, and quickly frozen in the liquid nitrogen for the sequencing process or other tests. All the operations about this process were performed on the ice, and the instruments used in the experiment were handled with diethyl pyrocarbonate (DEPC), autoclaved, and sterilized.

tiRNA and tRF sequencing

The total RNA was extracted from the hippocampus (3 mice/each group), NanoDrop ND-1000 (Thermo Fisher Scientific, ND-1000) was used to examine the purity and concentration of total RNA samples. Heavily RNA modifications were existed in the tiRNA and tRFs that disturb the construction of small RNA-seq library. We performed some treatments to total RNA samples before library preparation: for 3'-adaptor ligation, the 3'-cP (2',3'-cyclic phosphate) was removed to 3'-OH, 3'-aminoacyl (charged) was deacylated to 3'-OH, for 5'-adaptor ligation the 5'-OH (hydroxyl group) was phosphorylated to 5'-P, and demethylation of m1A and m3C for efficient reverse transcription. Then complementary DNA (cDNA) was synthesized with Illumina's proprietary RT primers and amplified using and amplification primers (Illumina, San Diego, CA, USA). Subsequently, extracting approximately 134–160 bp polymerase chain reaction (PCR) amplified fragments and purified with the polyacrylamide gel electrophoresis (PAGE) gel. Finally, quantifing the completed libraries with Agilent 2100 Bioanalyzer (Agilent Technologies, Santa Clara, CA, USA, G2938C). Afterward, sequencing was done on the Illumina NextSeq 500 system (Illumina, NextSeq 500) with NextSeq 500/550 V2 kit (Illumina, #FC-404-2005) according to the manufacturer's instructions by loading libraries onto reagent cartridge. The sequencing flow diagram is displayed in *Figure 1*.

tiRNA and tRF data analysis

After raw sequencing data was generated from Illumina NextSeq 500, some analysis were performed: aligning trimmed reads (trimmed 5', 3'-adaptor bases) to the mature tRNA sequences allowing for 1 mismatch, the reads that do

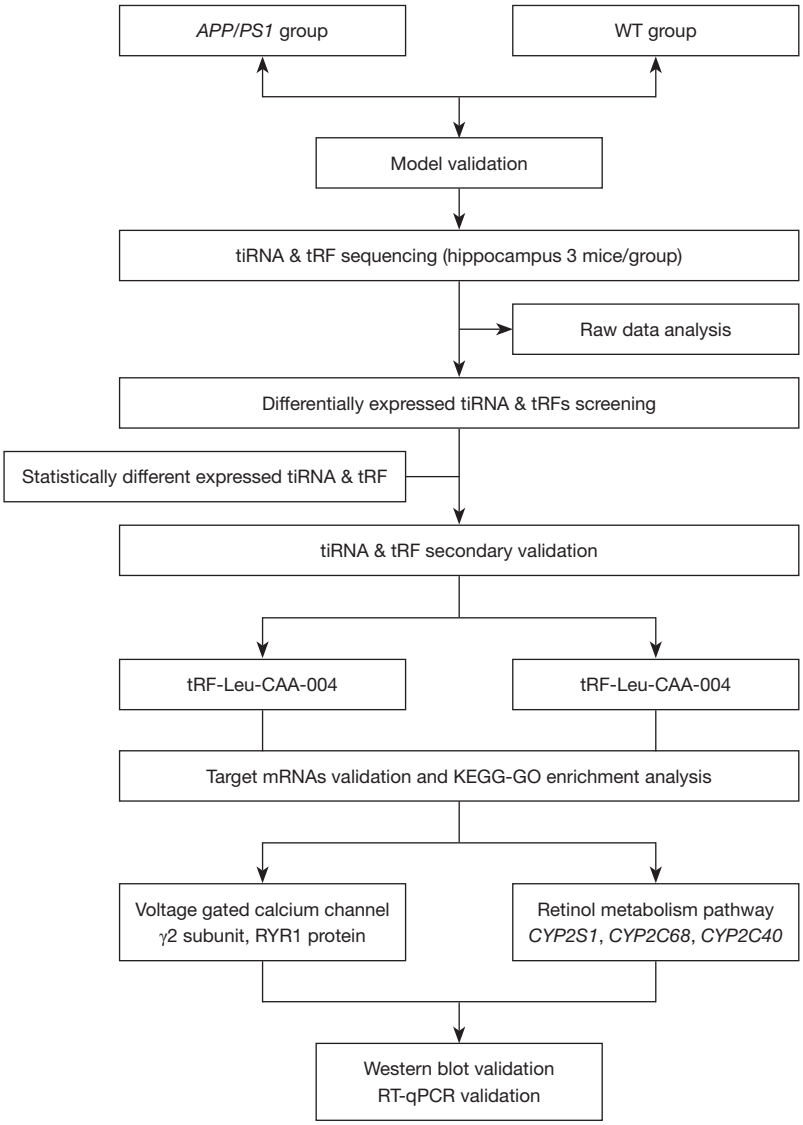

Figure 1 The workflow of the tiRNA and tRF sequencing. WT, wild type; mRNA, messenger RNA; KEGG, Kyoto Encyclopedia of Genes and Genomes; GO, Gene Ontology; RT-qPCR, real time quantitative PCR.

not map were then realigned to precursor tRNA sequences with bowtie software (34) allowing for 1 mismatch. After the alignment, the differentially expressed tiRNA and tRFs and expression profiling were calculated. The abundance of tiRNA and tRF was evaluated using their sequencing counts and was normalized as counts per million (CPM) of total aligned reads.

Then, the tiRNA the tRF are filtered if CPM less than 20 in all samples. For each tiRNA and tRF, the expression level was estimated using the mapped reads number and given an ID. The tiRNA and tRF ID was divided into four parts by the horizontal line, for example: "tRF-Gly-TCC-001". The following is a brief description of these fields: (I) tRF or tiRNA, the type of tiRNA and tRF; (II) type of amino acid; (III) type of anticodon; (IV) serial, the serial number of tiRNA & tRF derived from the tRNA of the same anticodon.

Differentially expressed tiRNA and tRFs analyses were performed with R package edgeR (35). Fold change (FC) (cut-off 1.5) and P value (cut-off 0.05) were used for screening differentially expressed tiRNA and tRFs.

Table 1 Primers used in qPCR analysis

Gene name	Primer sequence (5'-3')
U6	F: 5'-GCTTCGGCAGCACATATACTAAAAT-3'
	R: 5'-CGCTTCACGAATTTGCGTGTCAT-3'
tRF-Leu-CAA-004	F: 5'-ACAGTCCGACGATCGTCAGG-3'
	R: 5'-TCTTCCGATCTCTCGGCCA-3'
tRF-Thr-CGT-003	F: 5'-AGTCCGACGATCGCCCTCT-3'
	R: 5'-CGATCTAAATTCTTAAATCCACACG-3'
tRF-Val-AAC-030	F: 5'-TCTACAGTCCGACGATCGTTTCT-3'
	R: 5'-TCTGCGAGCGTGATAACCACT-3'
Cacng2	F: 5'-ATCTCCATGTACACCCTCAGTA-3'
	R: 5'-GTTATCCCTGTCCGAGTTGTAG-3'
RyR1	F: 5'-CTGGGCTATGGCTACAACATC-3'
	R: 5'-GACTGCTTCAAACTCGAAGTAC-3'
β-actin	F: 5'-CTACCTCATGAAGATCCTGACC-3'
	R: 5'-CACAGCTTCTCTTTGATGTCAC-3'
CYP2S1	F: 5'-AAGATGGCACAGGAGAAACAAG-3'
	R: 5'-CCCAGCAAACAGCAGGTATG-3'
CYP2C68	F: 5'-ATTTGCTCTCCTGCTCTTGATG-3'
	R: 5'-TTGTGTAAGGCATGTGGTTCC-3'
CYP2C40	F: 5'-GAAGGATTCCGGTTTTTGACAA-3'
	R: 5'-TCTTGCACTTTGTTCTCAATGG-3'

qPCR, quantitative polymerase chain reaction.

Validation by quantitative real-time qPCR

To further reconfirm the differentially expressed tiRNA and tRFs, we performed Real time Quantitative PCR (RT-qPCR) (3 mice/each group). Firstly, the hippocampus was homogenized in trizol (Invitrogen Life Technology, Carlsbad, CA, USA), then chloroform was added (Shanghai Chemical Reagents Co., Ltd., Shanghai, China) to separate the RNA, which was then transferred to the aqueous phase to include RNA to a new EP, isopropanol (Shanghai Chemical Reagents Co., Ltd.) was added to precipitate the RNA. The cells were then rinsed in 75% ethyl alcohol and water without Rnase to dissolve the RNA. Then, the RNA quality and concentration was detected with NanoDrop® ND-1000.

For tiRNA and tRFs, a rtStar™ tiRNA & tRFs pretreatment kit (Cat# AS-FS-005, Arraystar, Rockville, MA, USA) was used to remove some modifications and reverse transcription was performed with rtStar™ First-Strand cDNA Synthesis Kit (3' and 5' adaptor) (Cat# AS-FS-003, Arraystar) according to the manufacturer's instructions. Lastly, qPCR was performed with a ViiA 7 Real-time PCR System (Applied Biosystems, Waltham, MA, USA) and 2X PCR master mix (Arraystar) according to the manufacturer's protocol. For the target messenger RNAs (mRNAs), All-in-One™ First-Strand cDNA synthesis kit (Guangzhou Yijin Biological Technology Co., Ltd., Guangzhou, Guangdong, Cat# QP007) was used for the cDNA synthesis according to the manufacturer's instructions, then qPCR was performed with Mx3005P system and Blaze Taq™ SYBR Green qPCR Mix 2.0 (Guangzhou Yijin Biological Technology Co., Ltd., Cat# QP032). For the target mRNA real-time qPCR, the relative RNA expression was calculated by the $2^{-\Delta\Delta CT}$ method. We used U6 and β-actin as reference genes, and the primers used are listed in *Table 1*.

Target gene prediction

The tiRNA and tRFs contain sequences that might be complementary to the mRNA (36,37). Besides, it was reported that the tiRNA and tRFs could function as the miRNA that result in mRNA silencing (15,38). In this study, we used miRanda (https://www.mirandakerr.com/) and Target Scan (http://www.targetscan.org/vert_72/) to predict the target genes. Finally, the network illustration was visualized with Cytoscape software (version 2.8.3, https://cytoscape.org/).

Gene Ontology (GO) and Kyoto Encyclopedia of Genes and Genomes (KEGG) enrichment analysis

The GO project provides a controlled vocabulary to describe genes and gene product attributes in any organism (http://www.geneontology.org). Pathway analysis is a functional analysis mapping gene to KEGG pathways (in which the recommended P value cut-off is 0.05). We applied GO pathway analysis to the target genes of tiRNA and tRFs to find the changed mRNAs and pathways in *APP/PS1* mice.

Western blot

The hippocampus was used for western blot (5 mice/each group). The proteins were extracted with a Total Protein Extraction Kit (Applygen Technologies Inc., Beijing, China)

according to the manufacturer's instructions. Extracted protein concentration was texted with a bicinchoninic acid (BCA) Protein Assay Reagent Kit (Boster Biological Technology Co., Ltd.). A total of 25 μg protein was electrophoresed on the sodium dodecyl sulfate (SDS)-PAGE with electrophoresis apparatus (Beijing Liuyi Biotechnology Co., Ltd., Beijing, China); then the separated proteins were transferred onto a 0.22 μm polyvinylidene fluoride (PVDF) membrane (Millipore Corp., Burlington, MA, USA), followed by blocking with 5% nonfat dry milk in TBS with Tween 20 (TBST) (TBS: pH 7.4; NaCl 8 g; Tris 3 g dissolved with 1,000 mL distilled water) for 1 h at room temperature. Afterwards, the membrane was incubated with the primary antibodies at 4 ℃ overnight: anti-γ2 (1:800; Millipore Biotechnology), anti-RYR1 (1:500; Millipore Biotechnology), anti-$A\beta_{42}$ (1:500, Santa Cruz Biotechnology, USA), anti-CYP2S1 (1:500 Abcam, Cambridge, UK), anti-β-Tublin [1:2,000; Cell Signaling Technology (CST), Danvers, MA, USA], and anti-GAPDH (1:2,000; CST), which were diluted with TBST or 5% nonfat dry milk. The next day, incubating the membranes with fluorescent-labeled secondary antibodies (IRDye 800-conjugate goat anti-rabbit IgG or anti-mouse IgG, 1:5,000, Rockland Immunochemicals, Gilbertsville, PA, USA) for 2 h at room temperature. The membranes were then analyzed on an Odyssey infrared scanner (LI-COR Biosciences, Lincoln, NE, USA).

Vitamin A concentration analysis by liquid chromatography with tandem mass spectrometry

We tested the serum vitamin A concentration of *APP/PS1* mice and WT mice (10 mice/each group). The mice were anesthetized with chloral hydrate and then rotated by the tail in an upside position down to concentrate the blood to the head. The whiskers were cut with scissors, one eyeball was quickly removed, blood was collected into an EP tube, spun at 2,000 rpm/10 min, and the serum was collected.

The vitamin A concentration was tested with liquid chromatography with tandem mass spectrometry (LC-MS/MS) analysis on LC-20ADXR UPLC system (Shimadzu Corp., Kyoto, Japan) coupled to a 5500 Quadrupole TRAP® MS (AB Sciex, Foster City, CA, USA), which was operated with Analyst® 1.6.2 software (AB Sciex, USA). Nitrogen was used as the nebulizer (GS1), heater (GS2), and curtain (CUR) gas.

Statistical analysis

All results were presented as mean ± standard deviation (SD). The test results were analyzed by SPSS 22.0 (IBM Corp., Armonk, NY, USA) and Graph Pad Prism 7.0 (GraphPad Software, San Diego, CA, USA). Statistical comparisons were carried out with Mann-Whitney U test. All experiments were replicated at least 3 times. Statistical significance was considered when the P value was <0.05. The difference of the escape latency data in the MWM test was compared with one-way repeated measures analysis of variance (ANOVA). The western blot results were analyzed with Image J (https://imagej.nih.gov/ij/). The histograms were analyzed with GraphPad Prism 7. Principal component analysis (PCA), volcano plots, hierarchical clustering, scatter plots, Venn plots, and pie plots were performed in Perl or R environment for statistical computing and graphics of the expressed tiRNA and tRFs. All results were assessed by investigators who were blinded to the animal groups.

Results

The cognitive impairment validation

In the MWM acquisition trial (6 mice/each group), the *APP/PS1* mice showed a decreased spatial learning and memory ability as time elapsed compared with WT mice ($F=27.63$, $P<0.001$) (*Figure 2A*); however, the swimming speed of the two groups did not show a significant difference (*Figure 2B*). At the probe trial, when the platform was removed, the platform crossover number and the percentage of the time spent in the target quadrant were significantly decreased in *APP/PS1* mice that showed impaired spatial learning (*Figure 2C,2D*). From the mice swimming trajectory (*Figure 2E,2F*), we discovered that the *APP/PS1* mice swam more aimlessly and their swimming trajectories were scattered (*Figure 2E*), while the WT mice swim tracks were more concentrated around the removed platform (*Figure 2F*). All the mice used during the study were subjected to gene identification (*Figure 3A*). Besides, the male WT and *APP/PS1* mice were validated to ensure the cognitive impairment and pathological changes. Western blot (5 mice/each group) and immunofluorescence (5 mice/each group) revealed that the *APP/PS1* mice had apparently increased $A\beta_{1-42}$ in the hippocampus (*Figure 3B-3D*) which was consistent with the result of MWM. Above all, the *APP/PS1* mice successfully represented an AD model.

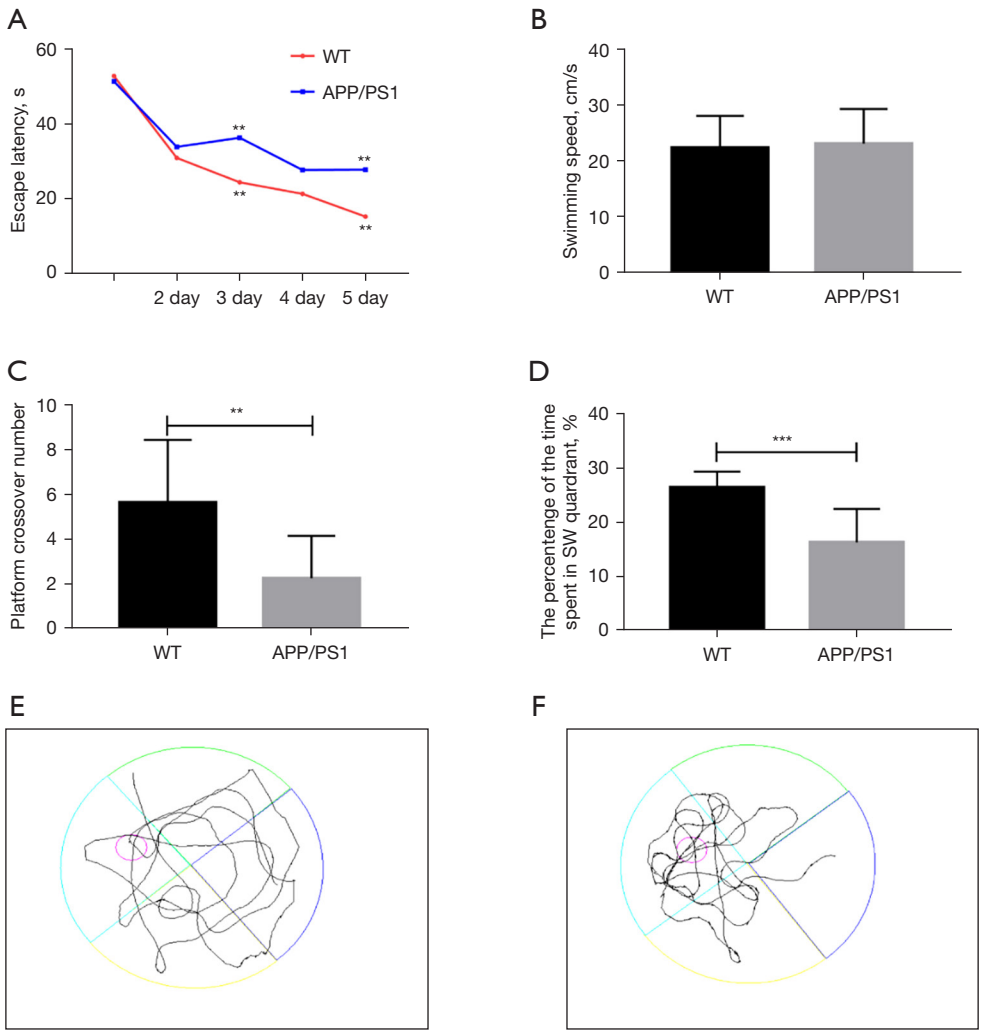

Figure 2 The *APP/PS1* mice showed impaired learning and memory in MWM (11-month-old *APP/PS1* and WT mice, 6 mice/each group). (A) The escape latency in the acquisition trial. (B) The average swimming speed between groups. (C) The number of crossings through the target quadrant (where the platform was previously located) in the probe test. (D) The percentage of time spent in the target quadrant in the probe trial. (E) *APP/PS1* and (F) WT representative path tracings during the probe trial. All data are presented as mean ± SD. **P<0.05, ***P<0.005 (n=6, one-way repeated measures ANOVA). MWM, Morris water maze; WT, wild type; SD, standard deviation; ANOVA, analysis of variance.

Preliminary analysis of tiRNA and tRF sequencing data

There were 44,742,669 raw sequencing reads after quality filtering (22,289,936 in the *APP/PS1* mice and 22,452,733 in the WT mice). The quality score Q is logarithmically related to the base calling error probability. To examine the sequencing quality, we used the proportion of bases (Q≥30, Q=30 indicated the incorrect base calling probability to be 0.001) numbers in two groups to represent the sequencing quality. The proportion of bases Q≥30 in two groups were all greater than 94%. After the sequencing reads were 5', 3'-adaptor trimmed, discarding reads length >40 nt or length <14 nt, we found 15,764,016 reads in *APP/PS1* and 15,664,828 in WT mice (3 mice/each group). The reads length was mainly distributed between 19–24 nt in the two groups (Figure S1).

After mapping with GtRNAdb (39) and tRNAscan-SE (40), there were 357,568 mature tRNA fragments in the *APP/PS1* group and 348,620 fragments in the WT group, a total of 151,439 precursor tRNA fragments in the *APP/*

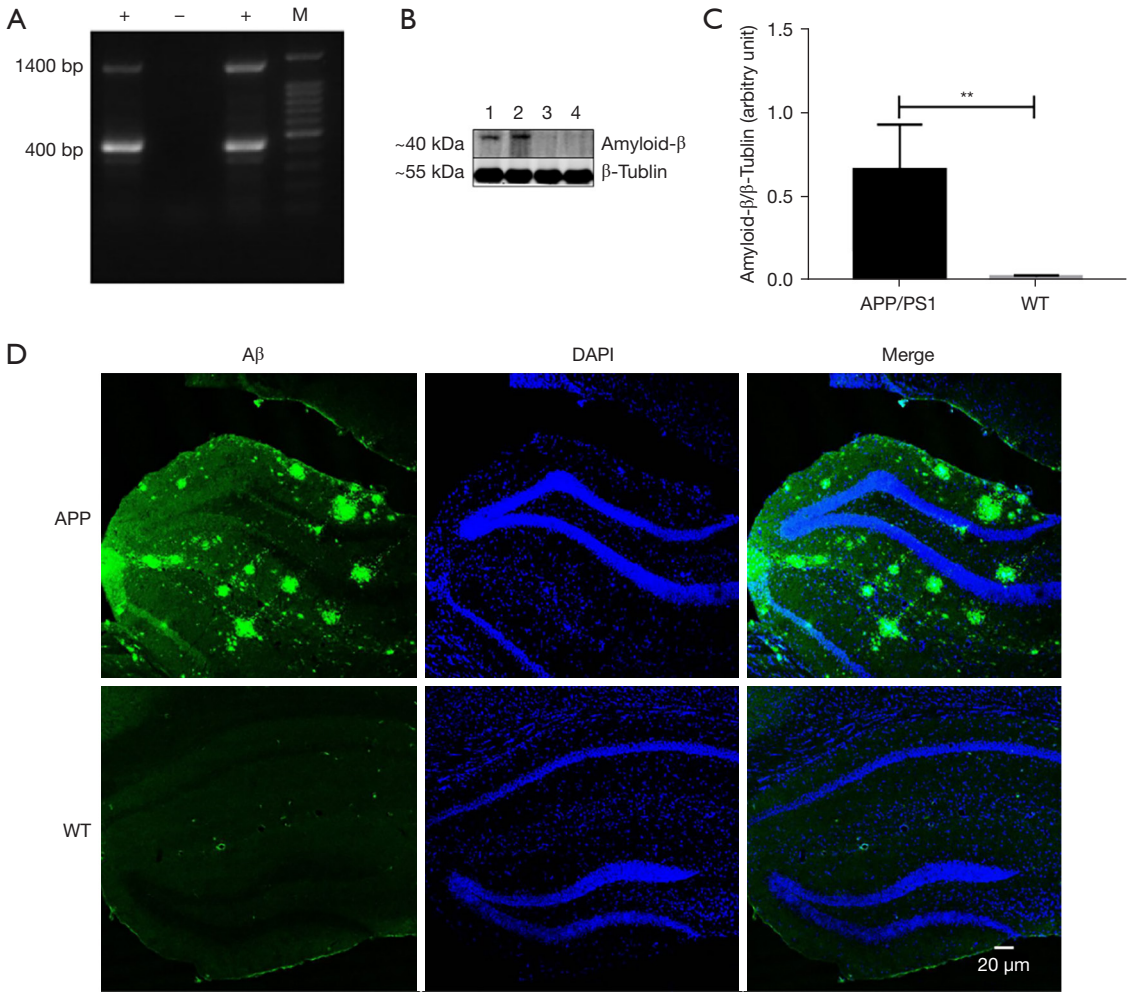

Figure 3 *APP/PS1* mice showed increased $A\beta_{1-42}$. (A) The result of *APP/PS1* gene identification, the positive results showed two bands at 400 and 1,400 bp which mark with "+" in (A), "M" denotes the band marker; (B) the western blot of $A\beta_{1-42}$, the β-Tublin was used as the internal reference, the first two columns (column 1 and 2) were *APP/PS1* mice, column 3 and 4 were WT mice; (C) the quantification of the $A\beta_{1-42}$ relative to the β-Tublin, mean ± SD, **P<0.05 unpaired *t*-test; (D) the upper row was from the CA1 area of *APP/PS1* mice, the lower row was from the WT mice. The green fluorescent represents the Aβ deposition, the blue fluorescent areas represent the nucleus (DAPI), (scale bar =20 μm). Aβ, amyloid-β; WT, wild type.

PS1 group and 152,731 in the WT group. The abundance of tiRNA and tRF were evaluated using their sequencing counts and were normalized as CPM of total aligned reads. The PCA is a kind of statistical method with unsupervised analysis so that reducing the large data sets dimensions. According to the expression, the PCA could well explore the classes of samples. We performed PCA with tRF and tiRNAs that had an ANOVA P value <0.05 on CPM value. The results from PCA showed a distinguishable tRF and tiRNA expression profiling between the *APP/PS1* group and WT group (*Figure 4*).

We screened the tiRNA and tRF so that the average CPM of each group was not less than 20 and separated the tiRNA and tRFs according to their tiRNA and tRF subtypes. The tiRNA and tRF subtypes distribution was similar in two groups. In the *APP/PS1* group, the tiRNA and tRF subtypes relative expression were: tRF-5c (27.1%), tRF-1 (20.48%), tRF-3a (15.2%), tRF-5a (12.56%), tRF-3b (9.47%), tRF-5b (7.49%), tiRNA-5 (5.95%), tRF-2 (2.44%), tiRNA-3 (1.1%). That in the WT group was tRF-5c (26.78%), tRF-1 (20.09%), tRF-3a (15.33%), tRF-5a (12.96%), tRF-3b (8.86%), tRF-5b (7.78%), tiRNA-5

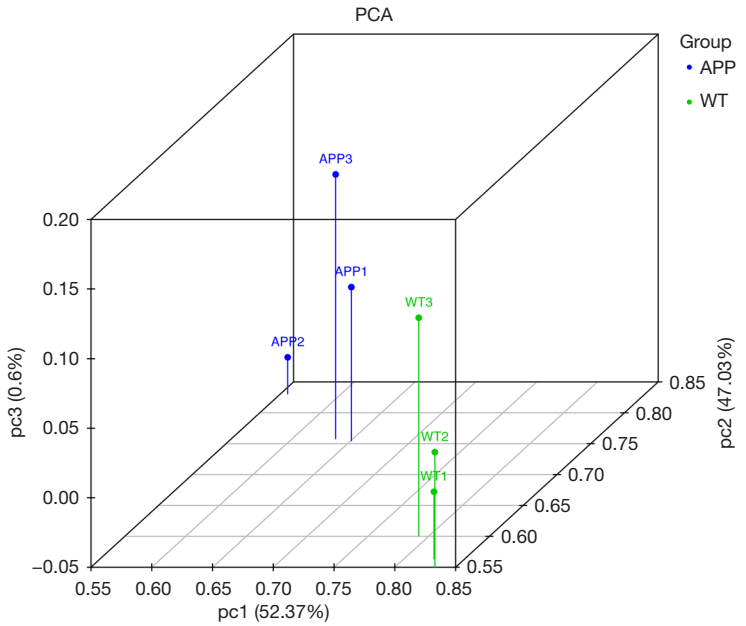

Figure 4 PCA. The three axes (X, Y, and Z) respectively represent three main factors affecting sample expression level. The blue and green dots represent the *APP/PS1* and WT samples, and the spatial position shows the main character of the sample. The space distance between the spots represents the similarity and difference of data size. PCA, principal component analysis.

(6.05%), tiRNA-3 (1.08%), and tRF-2 (1.08%) (*Figure 5A*). There were some slight differences between the two groups. In the *APP/PS1* group, the tRF-2 proportion was more than tiRNA-3 (2.44% and 1.1%, respectively), but in WT group, the tRF-2 and tiRNA-3 proportion was equal (1.08%). Besides, tRF-3b, tRF-1, and tRF-5c proportions in the *APP/PS1* group were slightly higher than those in the WT group, the tRF-5b, tRF-5a, and tRF-3a in the *APP/PS1* mice were lower in WT mice.

We then analyzed the distribution of tiRNA and tRF subtypes length: the length of tRF-1s were not fixed, fluctuated between 14–33 nt, but were mainly concentrated at 14, 20, and 27 nt, which may be related with the split site of pre-tRNA, as the split site was not fixed. The length of tiRNA-3 was mainly between 38–40 nt, tRF-5c were mainly present in 28–32 nt, tRF-5b were mainly between 22–24 nt, tRF-3b were mainly between 19–22 nt, tRF-3a were mainly between 17–18 nt, tRF-5a were mainly between 14–16 nt, and the tRF-2 expressions were relatively low, with only a few reads present at 14–15 nt. The tiRNA-5 were mainly between 34–35 nt, a slightly scattered tiRNA-5 at 33, 31, 27, and 20 nt, while the tiRNA-5 were also present in 30 nt in *APP/PS1* mice which were not in WT mice (*Figure 5B*).

The tRNA isodecoders share the same anticodon but have differences in their body sequence. The number of tiRNA and tRF subtypes that the average CPM was not less than 20 was counted against tRNA isodecoders. We can conclude from *Figure 5C* that there were some similarities between groups, the Valine (Val) and Glycine (Gly) derived tiRNA and tRFs were highly expressed in two groups; tiRNA-3 was only derived from Gly, Histidine (His), and Val tRNAs in the *APP/PS1* and WT groups; and tRNA-Arg was mainly producing tRF-1s and some tRF-3a. Some differences also existed between two groups. In the *APP/PS1* transgenic mice group, the tRNA-Asn (Asparagine) could produce the tRF-5c subtype, tRNA-Glu-CTC (Glutamic acid) could produce tRF-3a, tRNA-Phe (Phenylalanine) could produce tRF-1, tRNA-Ser-AGA (Serine) could produce tRF-5b, tRNA-Ser-CGA (Serine) could produce tRF-3b, tRF-5a, but this was not possible in the WT mice group. In the WT group, the tRNA-Gln-CTG (Glutamine) could produce tiRNA-5, tRNA-Gln-TTG could produce tRF-5b, tRNA-Gly-GCC could produce tRF-1, tRNA-His-GTG could produce the tRF-2, tRNA-Leu-AAG could produce tRF-2 and tRF-5b, tRNA-Leu-TAG could produce tRF-5b, and tRF-Thr-TGT (Threonine) could produce tRF-5c, which was not possible in the *APP/PS1* mice. This phenomenon further supports the hypothesis that tRFs are

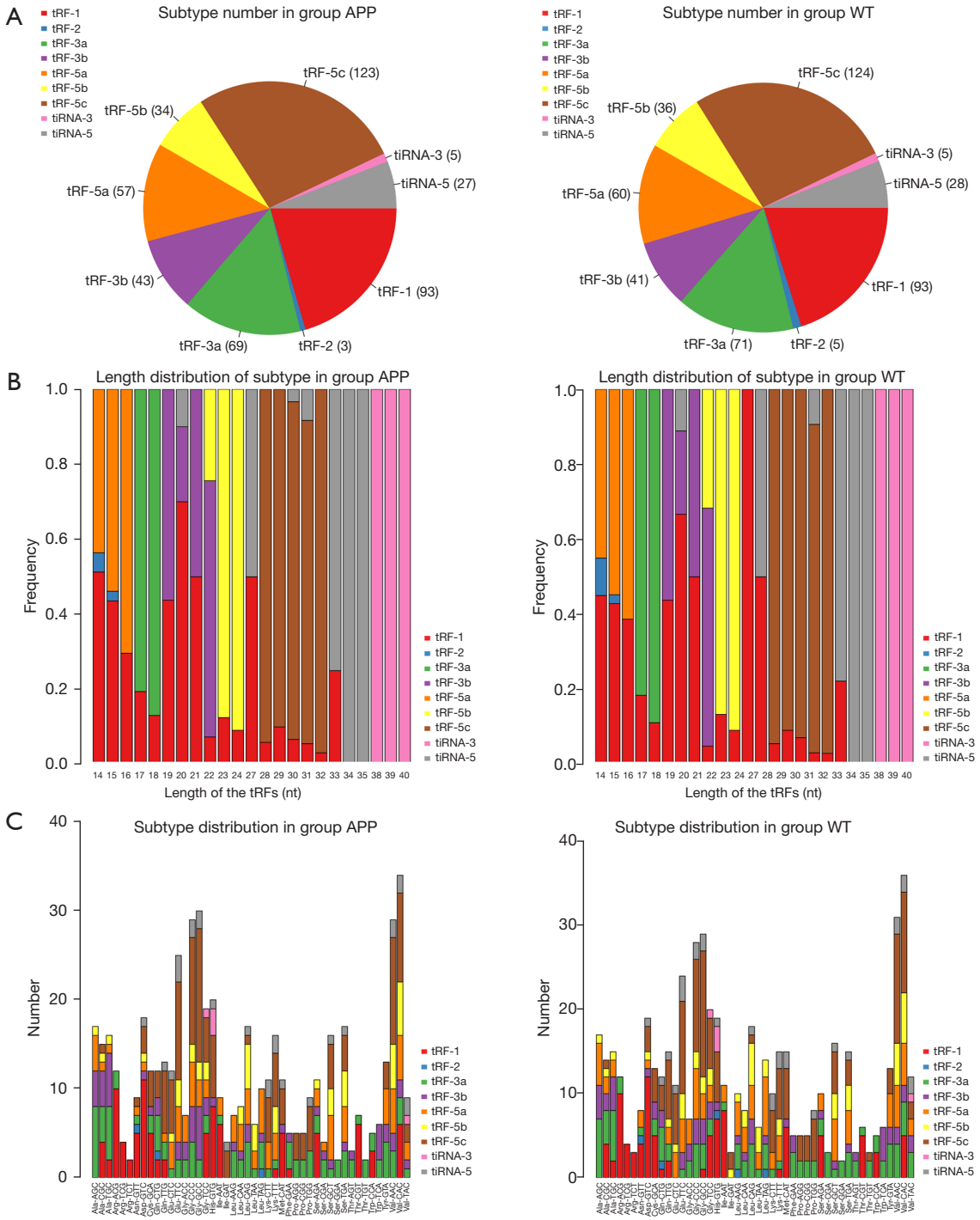

Figure 5 The expression profiles of tiRNA and tRF. (A) Pie chart of the distribution of tiRNA and tRF subtypes. The values in brackets represent the number of tiRNA and tRF subtypes. The color represents the tiRNA and tRF subtype. (B) The Frequency of subtype against length of the tiRNA and tRF. The X axes represent tiRNA and tRF length, Y axes show the frequency against length of the tiRNA and tRF subtype. Each tiRNA and tRF subtype with a indicated color in the right. (C) The subtype number of tiRNA and tRF against tRNA isodecoders. The X axes represent tRNA isodecoders, Y axes show the tiRNA and tRF subtypes number against tRNA isodecoders. The color represents the tiRNA and tRF subtype.

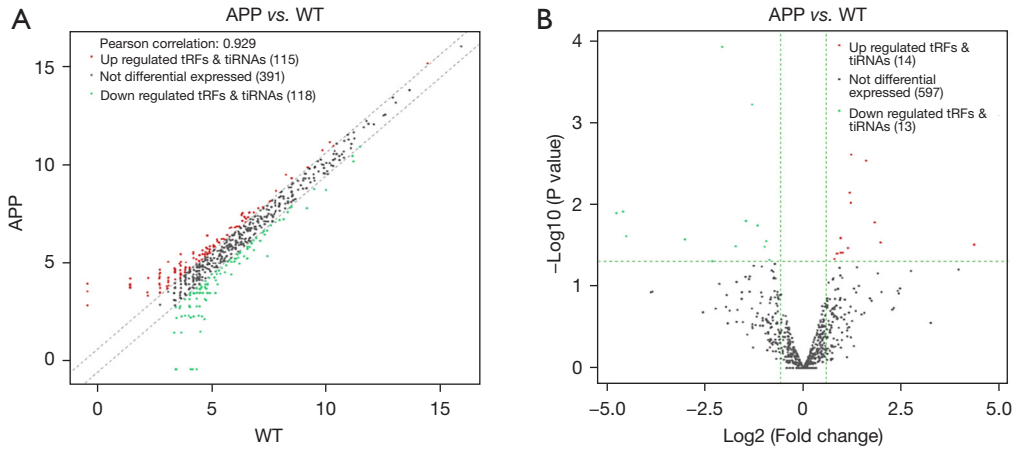

Figure 6 The differentially expressed tiRNA and tRFs between *APP/PS1* mice and WT mice. (A) The scatter plot between two groups for tiRNA and tRFs in *APP/PS1* mice and WT mice. All tiRNA and tRFs were plotted with CPM values. In the scatter plot, the values on the X and Y axes represent the averaged CPM values of each group (log2 scaled). The red dots (up-regulation) and green dots (down-regulation) represent more than 1.5-FC between *APP/PS1* and WT mice groups. Gray dots indicate no expressing change of tiRNA and tRFs between groups. (B) The volcano plot of tiRNA and tRFs in *APP/PS1* mice and WT mice. In the volcano plot, the values on the X axes represent the log2 transformed FC, and values on the Y axes represent the –log10 transformed P values between the two groups. The red and green dots indicate statistically significant differentially expressed tiRNA and tRFs, P value ≤0.05, FC ≥1.5 (green: down-regulated; red: up-regulated). Gray dots indicate no expressing change. FC, fold change; WT, wild type; CPM, counts per million.

non-random, stable products derived from specific tRNA and pre-tRNAs. In other words, the distribution of mapped reads appeared as non-random as those of miRNAs, strongly suggesting that their source was not indiscriminate degradation but rather a targeted biological process.

Altered expression profiles of tiRNA and tRFs in APP/PS1 transgenic mice

Based on alignment statistical analysis, 624 differentially expressed tiRNA and tRFs were detected between two groups and used for subsequent analyses (*Figure 6A*). Among the 624 differentially expressed tiRNA and tRFs, 27 were statistically significantly different (P<0.05). The differentially expressed tiRNA and tRFs with significant differences included 14 up-regulated and 13 down-regulated (FC >1.5, P<0.05) (*Figure 6B*), among which most came from tRF-5 category (Tables S1,S2). Among all the differentially expressed tiRNA and tRFs, There were 417 tiRNA and tRFs among the two groups that the CPM of each tiRNA and tRF was more than 20; there were 46 tiRNA and tRFs that the CPM values were more than 20 in WT group while less than 20 in APP group, 37 in *APP/PS1* group were more than 20 while less than 20 in WT group (*Figure 7A*); among all the differentially expressed tiRNA and tRFs, 87 were already known tRFs from tRFdb, and the others were detected in the current study (*Figure 7B*). Hierarchical clustering is one of the most widely used clustering methods for analyzing tiRNA and tRFs expressing data. Cluster analysis was used to arrange samples into groups based on the tiRNA and tRFs expressing level (CPM values), which allowed us to hypothesize the relationships among samples. The two groups could be clustered into two branches which manifest the satisfactory replication and representativeness of the *APP/PS1* group and WT group (*Figure 8*).

The tRF and tiRNA validation and target gene prediction

For further confirm the differentially expressed tiRNA and tRFs, we selected some tiRNA and tRFs for qPCR testing to further validate the high-throughput results (3 mice/each group), the primers of which are presented in *Table 1*. The screening criteria for tiRNA and tRFs of interest followed the principle that there were little differences in the CPM values within the WT and *APP/PS1* groups, and the CPM values in the two groups were relatively hign and with a difference between the two groups. We finally selected three tRFs: up-regulated tRF-Val-AAC-030 and tRF-Thr-CGT-003, and down-regulated tRF-Leu-CAA-004.

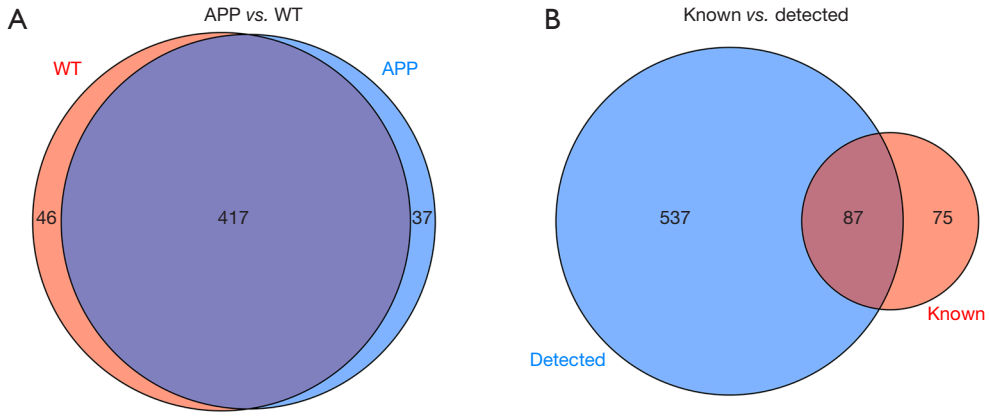

Figure 7 Venn diagram of tiRNA and tRFs in *APP/PS1* mice and WT mice. (A) Venn diagram shows the commonly expressed and specifically expressed tiRNA and tRFs. This diagram shows 417 tiRNA and tRFs that commenly expressed in both groups and 37 specific tiRNA and tRFs in *APP/PS1* group and 46 in WT group. (B) The number of tiRNA and tRFs which were already known in the tRFdb (87 tiRNA and tRFs) and detected only in this study (537 tiRNA and tRFs). This diagram shows the number of tiRNA and tRFs collected in the tRFdb and detected in this project. WT, wild type.

As a result, tRF-Thr-CGT-003 and tRF-Leu-CAA-004 passed the validation (P<0.005 and P<0.05, respectively). The structural and functional properties of tiRNA and tRFs resemble the miRNA, tiRNA and tRF can pair with the mRNA in the "seed" region and regulate the protein translation like miRNA (37). We then executed target gene prediction for tRF-Thr-CGT-003 and tRF-Leu-CAA-004 according to the miRNA information in the miRBase using the miRanda and TargetScan algorithms. As a result, we found a total of 236 target mRNAs for tRF-Thr-CGT-003 and 183 target mRNAs for tRF-Leu-CAA-004 for subsequent analysis.

Functional enrichment analysis

According to the predicted target mRNAs of tRF-Thr-CGT-003 and tRF-Leu-CAA-004, GO and pathway analysis was performed, mainly concentrating on calcium dysregulation and retinol metabolism. As a GO result, we found several calcium dysregulation related terms: including voltage-gated calcium channel activity (GO: 0005245), and calcium ion transmembrane transport (GO: 0070588). For KEGG analysis, we found several calcium dysregulation-related mRNA denotes: including *CACNG2* in the MAPK signaling pathway (mmu04010), oxytocin signaling pathway (mmu04921), and *RYR1* gene in the pathways of Apelin signaling pathway (mmu04371), circadian entrainment pathway (mmu04713), and long term depression pathway (mmu04730). Calcium is an indispensable factor for the pathogenesis of AD, its action can spread from the plasma membrane to the endoplasmic reticulum and mitochondria (41), so the calcium balance is important for AD. In the KEGG enrichment pathways, the retinol metabolism pathway (mmu00830) was most significantly changed in *APP/PS1* mice (P=3.14297E–08), among which *CYP2C40*, *CYP2C68*, and *CYP2S1* were the target genes of tRF-Leu-CAA-004. Above all, we speculated that tiRNA and tRF may have regulated the calcium dysregulation and retinol metabolism post-transcriptionally in the *APP/PS1* mice, we then observed the target genes of calcium regulation and retinol metabolism of tRF-Thr-CGT-003 and tRF-Leu-CAA-004. Finally, we focused on the *CACNG2*, *RYR1*, and *CYP2C40*, *CYP2C68*, *CYP2S1* genes, respectively.

The CACNG2 and RYR1 changes in APP/PS1 transgenic mice

The *CACNG2* gene encodes the voltage-gated calcium channel γ2 (γ2) subunits, which is a 4 transmembrane domains protein (42). The *RYR1* gene encodes the ryanodine receptor 1 protein (RyR1) which is a calcium release channel on endoplasmic/sarcoplasmic reticulum (ER/SR) (43). To further verify the regulation function of tiRNA and tRF in the *CACNG2* and *RYR1*, we performed the western blot (5 mice/each group) and RT-qPCR

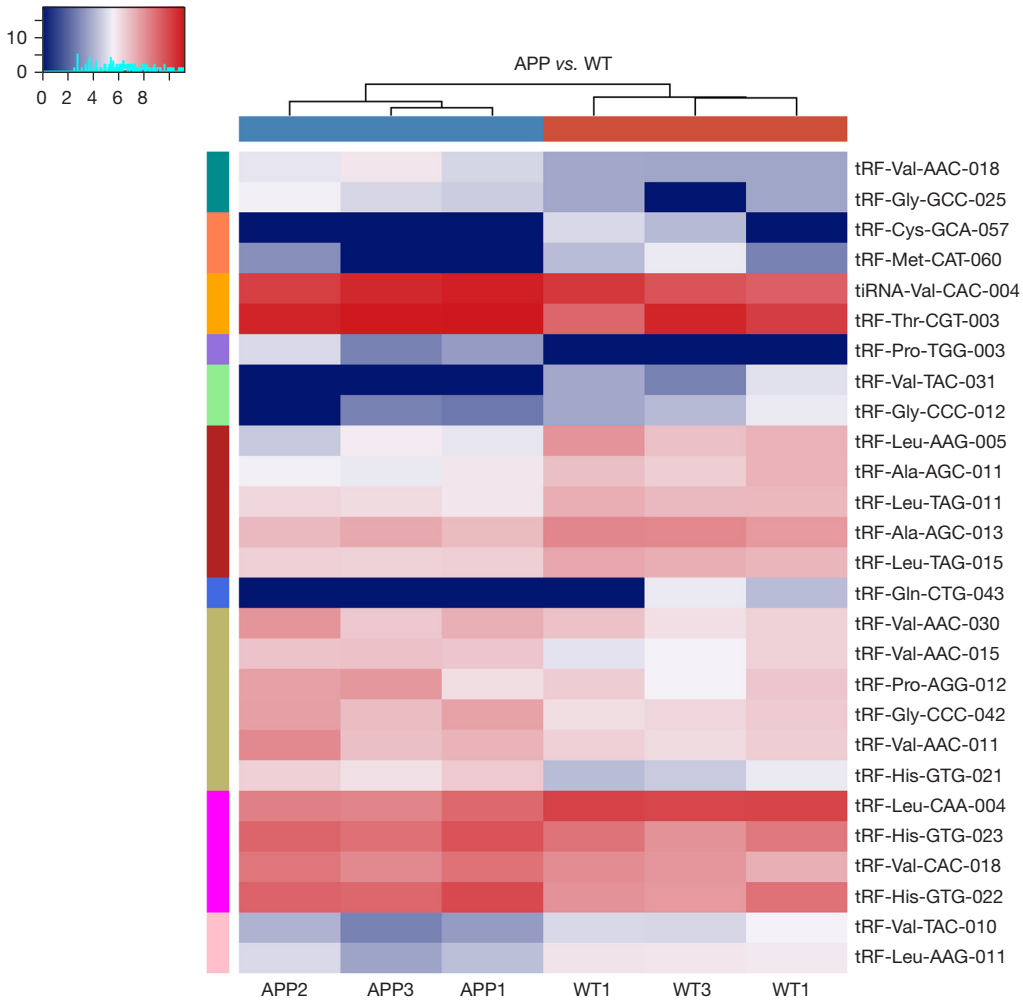

Figure 8 The unsupervised hierarchical clustering heatmap for tiRNA and tRFs in *APP/PS1* mice and WT mice. The panel color represents the relative expression level (log2-transformed). The expression level which below the mean was represent with blue color, and the expression level above the mean was shown with red. The colored bar at the top shows the sample groups, the bar at the left side represent the divisions which were performed with K-means. WT, wild type.

(5 mice/each group) (primers were presented in *Table 1*) analysis on the hippocampus from the translation and transcription levels. From the protein expression level, the γ2 subunit and RyR1 proteins in the hippocampus all increased obviously (*Figure 9A,9B*) (P<0.05). Meanwhile, the expressions of *CACNG2* and *RYR1* mRNAs increased significantly in *APP/PS1* transgenic mice compared with the WT mice (P<0.05) (*Figure 9C*) which was consistent with the western blot results, indicating that tRF-Leu-CAA-004 regulates the RYR1 protein and tRF-Thr-CGT-003 contributes to γ2 regulation through regulating the *RYR1* mRNA and *CACNG2* mRNA. In summary, tRF-Thr-CGT-003 and tRF-Leu-CAA-004 may participate in the regulation of voltage-gated calcium channel γ2 subunit and RyR1 proteins in *APP/PS1* mice.

Vitamin A in the APP/PS1 mice and WT mice

From the target mRNAs enrichment results, we also selected the retinol (vitamin A) metabolism pathway for further validation. Serum vitamin A concentration was tested with LC-MS/MS, which showed the concentration in *APP/PS1* and WT groups (10 mice/group) as 0.431±0.0248 and 0.243±0.0359 mg/L, respectively (*Figure 10A*). Retinol in *APP/PS1* mice was significantly higher than in WT mice. Retinoic acid is derived from vitamin A, which is the active

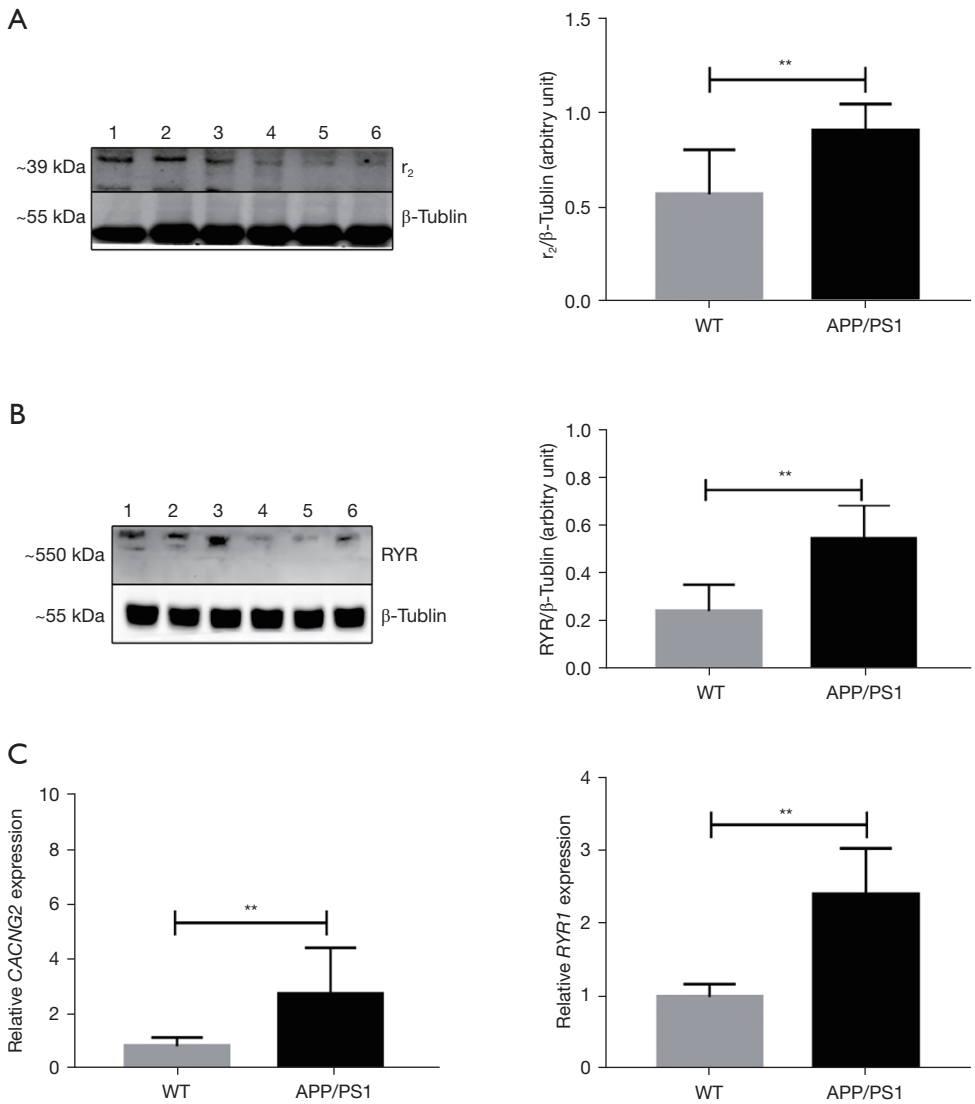

Figure 9 The *CACNG2* and *RYR1* expressions at the mRNA and protein levels. (A) and (B) the γ2 and RYR1 protein expression between the *APP/PS1* mice and WT mice. On the left, lane 1,2,3 are the *APP/PS1* mice, lane 4,5,6 are WT mice, the β-Tublin were used as the internal reference. The right columns were the quantification of γ2 and RYR1 proteins expression relative to the β-Tublin, mean ± SEM, (n=3, **P<0.05, *t*-test). (C) The *CACNG2*, *RYR1* mRNA expression levels, the β-actin were used as the internal reference. Mean ± SEM, (n=3, **P<0.05, *t*-test). mRNA, messenger RNA; SEM, standard error of the mean; WT, wild type.

metabolite, therefore, the increased vitamin A may have resulted in more retinoic acid in *APP/PS1* mice.

The change of CYP2S1, CYP2C68, and CYP2C40 between APP/PS1 mice and WT mice

Retinol was first metabolized to retinal, and then further metabolized to retinoic acid. The *CYP2S1*, *CYP2C68*, *CYP2C40* were shown to be metabolic enzymes of retinoic acid. In *APP/PS1* mice, *CYP2S1*, *CYP2C68*, and *CYP2C40* mRNA decreased significantly with qPCR (5 mice/each group) (*Figure 10B-10D*), the CYP2S1 protein was also decreased in *APP/PS1* mice with western blot (5 mice/each group) (*Figure 10E,10F*), which was consistent with the qPCR results. The decreased *CYP2S1*, *CYP2C68*, and *CYP2C40* may have been a compensation mechanism to reduce the metabolism of the retinoic acid in *APP/PS1* mice.

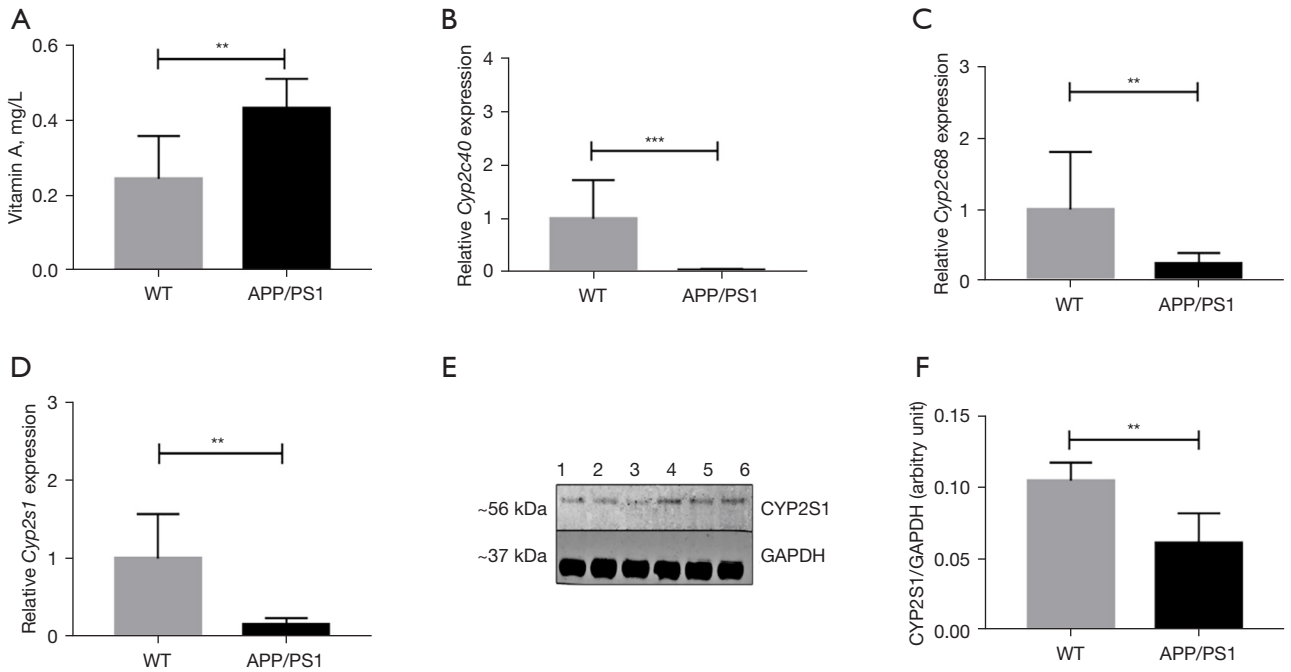

Figure 10 Vitamin A metabolism and tcytochrome P450 expression between *APP/PS1* mice and WT mice. (A) The vitamin A concentration between *APP/PS1* mice and WT mice (n=10, **P<0.05, *t*-test). (B-D) are the relative *CYP2S1*, *CYP2C68*, and *CYP2C40* mRNA expression between *APP/PS1* mice and WT mice. (E) The *CYP2S1* protein expression between the *APP/PS1* mice and WT mice. In the left, lane 1, 2, and 3 are *APP/PS1* mice, lane 4, 5, and 6 are WT mice, the GAPDH were used as the internal reference. (F) The quantification of *CYP2S1* proteins expression relative to the GAPDH, mean ± SEM, (n=3, **P<0.05, ***P<0.01, *t*-test). WT, wild type; SEM, standard error of the mean.

Discussion

APP/PS1 transgenic mice display an earlier onset and a more rapid rate of pathogenesis than monogenic lines, both in terms of amyloid accumulation and cognitive impairment (44). In our research, the mice were tested with MWM and Aβ expression, which showed significantly increased Aβ deposition and cognitive impairment in *APP/PS1* mice, which validated that the AD model has been successfully established. We further executed a tiRNA and tRF sequencing between *APP/PS1* transgenic mice and WT mice. As a result, a total of 27 statistically differentially tiRNA and tRFs were screened, among which 14 were up-regulated and 13 down-regulated. From these, we selected 3 tiRNA and tRFs for qPCR validation, and 2 tiRNA and tRFs were passed. Then, GO and KEGG enrichment analyses were processed to the predicted target mRNAs of tRF-Thr-CGT-003 and tRF-Leu-CAA-004. It was revealed that tRF-Thr-CGT-003 belonged to tRF1 and tRF-Leu-CAA-004 belonged to tRF-5. Additionally, tRF-Thr-CGT-003 was up-regulated and the target *CACNG2* mRNA level increased in qPCR, the γ2 protein (CACNG2 coding protein) showed an increased trend, indicating that the tRFs could potentially promote protein expression by increasing the *CACNG2* mRNA level. The tRF-Leu-CAA-004 was down-regulated in the *APP/PS1* mice, the target *RYR1* mRNA level was increased compared to the control group, and the target protein (RYR1 protein) was increased, which indicated that the tRF may inhibit the protein expression through inhibiting the *RYR1* mRNA, whereas the target mRNA *CYP2S1*, *CYP2C68*, and *CYP2C40* were decreased in mRNA level and protein level in *APP/PS1* mice. The two tRFs regulation trends were absolute opposites and the tRF-Leu-CAA-004 showed different regulation trends to the target mRNAs between *RYR1* and *CYP2S1*, *CYP2C68*, and *CYP2C40*.

Among the 27 differentially expressed tiRNA and tRFs, 8 tRFs were derived from tRF-Val, the $tRNA^{Val}$ derived fragments reported could regulate the Wnt/β-Catenin signaling pathway (45), which could inhibit Aβ production and Tau protein hyperphosphorylation in AD (46). Mo *et al.* reported that tRNA-Val-AAC and tRNA-Val-CAC could attenuate the THBS1/TGF-β1/Smad3 axis (47)

which could inhibit the inflammatory process in the central nervous system (CNS) (48), the two tRF fragments were up-regulated in *APP/PS1* mice. Through analyzing the target mRNAs of all differentially expressed tiRNA and tRF with GO enrichment, we found there were 24 target mRNAs which take part in the learning and memory biological process (GO: 0007611, $P=5.41\times10^{-5}$), 26 mRNAs take part in the synapse organization (GO: 0050808, P=0.0002), 24 mRNAs take part in the cognition biological process (GO: 0050890, P=0.0003), 48 mRNAs take part in the synaptic transmission (GO: 0007268, GO: 0098916, GO: 0099537, GO: 0099536, all with P<0.001), 15 mRNAs take part in the learning process (GO: 0007612, P=0.0007), some mRNAs also take part in the glutamatergic synaptic transmission (GO: 0035249), apoptotic process (GO: 0006915), regulation of axonogenesis (GO: 0050772), glutamate receptor signaling pathway (GO: 0007215), membrane hyperpolarization (GO: 0060081), postsynaptic chemical synaptic transmission (GO: 0099565), regulation of postsynaptic membrane potential (GO: 0060078), regulation of neurotransmitter transport (GO: 0051588), synaptic assembly (GO: 0007416), long term synaptic depression (GO: 0060292), regulation of neurotransmitter secretion (GO: 0046928), regulation of neuronal synaptic plasticity (GO: 0046928), regulation of neuronal synaptic plasticity (GO: 0048168), and Aβ metabolic process (GO: 0050435), all with P<0.05. From the KEGG enrichment pathways, steroid hormone biosynthesis (mmu00140, $P=1.12\times10^{-7}$), MAPK signaling pathway (mmu04010, P<0.05), GABAergic synapse (mmu04727, P<0.05), JAK-STAT signaling pathway (mmu04630, P<0.05), and long-term depression (mmu04730, P<0.05) were all shown to participate in the pathogenesis of AD (49-52). The above biological processes and pathways were all related to the AD pathology, which further supported that the tRFs were closely related with the progression of AD.

In our study, the differentially expressed tiRNA and tRFs were mainly tRFs, especially tRF-5s. The lack of tiRNAs may be due to the tiRNAs are mainly produced under stress conditions, such as hypoxia and sex hormone stimulation (53). So far, most research has mainly focused on the protein inhibition function of tRFs, which has mainly been restricted to the tRF5s (54). Although some tRFs inhibit the protein expression only to their target genes, some tRFs have also been shown to play a role in global translation repression. In archaeon *haloferax volcanii*, a $tRF\text{-}5^{Val}$ could target the small ribosomal subunit thus reduce protein synthesis by interfering with peptidyl transferase (55). Sobala *et al.* reported that tRFs required a conserved "GG" dinucleotide for inhibitory effects on global translation. As random sequences contain "GG" at positions 17–18 or 18–19 in tiRNA and tRFs, it could function in global translational modulation (54). Besides, other mechanisms were identified, such as interfering with cap-binding eIF4F complex (56), associate with YB-1 and induce the stress granules (SGs) (57), bind to argonaute proteins and competes for its corporation into RISC complex (58), displace the eIF4G/eIF4A from mRNA in a phospho-eIF2α-independent assembly of SGs (56), and so on. In our study, the down-regulated tRF-Leu-CAA-004 (tRF-5a) resulted in the increasing target gene *RYR1* mRNA and RYR1 protein which may be through the above mechanism, but the detailed mechanisms require further study.

Some tRFs have also been found to be regulators of rRNA and promote protein biogenesis (53). Kim *et al.* reported that LeuCAG 3'tRF could directly interact with ribosomal protein mRNAs (RPS28 and RPS15) to enhance their translation and ultimately increase the number of ribosomes and increase the protein synthesis (36). Fricker *et al.* reported that in *Trypanosoma brucei*, $tRNA^{Thr}$ 3'half (tiRNA-3) derived from 3' fragment which cleaved at the anticodon, a ribosome-associated ncRNA could be associated with ribosomes and polysomes, and could promote translation by facilitating mRNA loading. Knockdown of the tRNAThr 3'half could mitigate this stimulatory effect (59). From the above two studies, the tRFs proceeded the protein expression mainly through promoting the synthesis of ribosomes or through facilitating mRNA loading on ribosomes. In our study, we found that the increased tRF-Thr-CGT-003 may promote *CACNG2* mRNA and γ2 translation, and the decreased tRF-Leu-CAA-004 may control the *CYP2S1*, *CYP2C68*, and *CYP2C40* mRNAs and protein expression.

Calcium dysregulation has been deeply studied in AD. This pathogenesis is a complicated network which involves a number of channel proteins. In plasma membrane, Aβ and Tau could interact with the voltage-gated Ca^{2+}-influx channels (VGCC) and inhibit the Ca^{2+}-efflux ATPase or exchangers which leads to an elevated intracellular Ca^{2+} $[(Ca^{2+})_c]$ (41). Structurally, VGCC are heteromeric proteins composed of a pore-forming α1 subunit, as well as the auxiliary subunits: α2δ, β, and γ(γ1–γ8) (60). In ER/SR, RYR2 isoform, a Ca^{2+} release channel which has 3 isoforms (RYR1–RYR3), increased in 3xTg-AD mice at pre-symptomatic ages which evoked increased calcium release (61-63). Besides, enhanced inositol

1,4,5-trisphosphate receptor (IP3R)-mediated Ca^{2+} release could further aggravate Ca^{2+} disorder (41). In mitochondria, the increase of Ca^{2+} from ER to mitochondria through mitochondrial-associated ER membrane (MAM) (63) and the decrease of Ca^{2+} efflux from mitochondria through mitochondrial Na^{+}/Ca^{2+} exchanger (NCLX) (64) results in mitochondrial Ca^{2+} overload, and the opening of mitochondrial permeability transition pore (mPTP), which further leads to elevated reactive oxygen species (ROS) generation and the activation of apoptosis (65). For different VGCC subunits, the α1 was the central subunit, which determines the major characteristics of the calcium current to a great extent (42). The auxiliary subunits β and α2δ act as positive regulators of VGCC current, which could enhance the activation and/or opening probability of calcium channels (66-68). However, functional studies have revealed inhibitory effects of γ2 on neuronal calcium channels, co-expression of CaV2.2 with γ subunit could cause down-regulation of channel expression and decreased current amplitudes (69,70), whose expression in AD have not yet been studied; however, we first observed the increased γ2 unit in *APP/PS1* mice. In the mid- to late-stage of AD, increased γ2 may be a compensatory mechanism to counteract the overactive calcium influx. Besides, the γ subunits not only interact with calcium channels, but also with some other proteins as well (42). Some research discovered that γ2 could take part in the synaptic targeting and membrane trafficking of the AMPA receptor (AMPA-R) subunits (GluR1, GluR2, and GluR4) and further enhanced AMPA-R current, thus increasing the rate of channel opening (42). The AMPA-R are crucial for synaptic plasticity and higher brain function. Both Aβ and increased $[Ca^{2+}]_c$ could induce the AMPA-R internalization with a decrease in cell-surface AMPA-R expression thus impairing synaptic function (71,72). The increased γ2 expression may be a compensation for the decreased cell-surface AMPA-R expression. Besides, Milstein *et al.* reported that overexpression of γ2 could reduce the mEPSP amplitude and slow the decay speed (73). Besides, from the GO enrichment results, we found that *CACNG2* also took part in regulation of the glutamate receptor signaling pathway (GO: 1900449). In 11.5–12-month-old *APP/PS1* mice, we detected up-regulated tRF-Thr-CGT-003 and down-regulated tRF-Leu-CAA-004, and, as a result, their target proteins: γ2 and RYR1 increased due to the tRF-Thr-CGT-003 and tRF-Leu-CAA-004 regulation. The increased RYR1 could result in increased Ca^{2+} efflux from ER/SR to plasma, while the increased γ2 protein could inhibit the VGCC and reduce the Ca^{2+} influx, which may be a compensation for the plasma Ca^{2+} increasing.

In the retinol metabolism pathway, the serum retinol (vitamin A) concentration was increased, the metabolic enzymes *CYP2S1*, *CYP2C68*, and *CYP2C40* of retinal acid (74) were all decreased in mRNA level and protein level. Vitamin A is essential for vision, reproduction, growth and differentiation, and maintenance of the general health. Retinoic acid is the active retinoid form responsible for mediating most of the nonvisual functions (75); Aβ can down-regulate the retinoic acid receptor (RAR) α signaling and inhibit the synthesis of the ligand-retinoic acid (76). Retinoic acid could inhibit the aggregation of Aβ25-35 through the specific binding of retinoic acid to the C-terminal portion of Aβ, thus decreasing cellular toxicity (77). The *APP/PS1* transgenic mice treated with retinoic acid manifested a robustly decreased Aβ deposition and Tau phosphorylation (78). We proposed that the increased vitamin A and decreased *CYP2S1*, *CYP2C68*, and *CYP2C40* were compensating for the increased cerebral Aβ deposition, and were intended to increase the relatively retinoic acid in the brain. Some of our findings were contradictory to previous studies. Some researchers have reported that the vitamin A levels in AD patients were significantly decreased (79,80); however, we found that the AD patients' were all above 70 years old, whereas our mice were 11.5–12 months, which equated to quinquagenarian mice. We thought that the increased vitamin A may be compensatory mechanism to the retinoic acid. Some researchers have supported that the retinoic acid availability in the brain of AD is influenced, the retinoid hypofunction and the transportation impairment existed in the late onset AD. They proposed that targeting the retinoic acid receptors or cytochrome P 450 enzymes may prevent or decrease amyloid plaque formation (81), which was consistent our hypothesis. Regrettably, we were unable to test the retinoic acid concentration in the mice due to technical reasons.

Limitation

In our study, we determined the differentially expressed tiRNA and tRFs between the *APP/PS1* group and WT group, and found that tRF-Thr-CGT-003 and tRF-Leu-CAA-004 may regulate the calcium regulation of related proteins and the retinol metabolism. However, there were some limitations to our research. Firstly, we just tested the regulative function of tRF-Thr-CGT-003 and tRF-Leu-CAA-004 on target mRNAs and protein levels, but

the detailed mechanisms between the tRFs and the target mRNAs need further exploration. Secondly, we just observed 11.5–12-month-old mice; the tiRNA and tRF expression and their related target mRNAs expression are a dynamic process, it would be more beneficial to observe the early stage and the late stage related variation of *APP/PS1* mice in the future study.

Conclusions

In general, our research first studied the tiRNA and tRFs regulation in 11.5–12-month-old AD model of *APP/PS1* mice, and found that tRFs could regulate the calcium-related proteins and the retinol mechanism-related proteins, which may provide us a therapeutic target for the treatment of AD. We found the expression change of some tiRNA and tRFs in *APP/PS1* mice, which may be closely connected with the Aβ production, but whether the tiRNA and tRFs expression change is a direct cause of Aβ production or just a secondary change of Aβ production still requires further research. There are hundreds of different tiRNA and tRFs, their function has been studied by many researchers, yet we still have actually only scratched the surface of their mechanisms. Ongoing efforts are required to uncover the physiological roles of these tiRNA and tRFs.

Acknowledgments

Funding: This research was supported by the Key Project of Natural Science Foundation of Hebei Province (H2018206361).

Footnote

Reporting Checklist: The authors have completed the ARRIVE reporting checklist. Available at https://dx.doi.org/10.21037/atm-21-4318

Data Sharing Statement: Available at https://dx.doi.org/10.21037/atm-21-4318

Conflicts of Interest: All authors have completed the ICMJE uniform disclosure form (available at https://dx.doi.org/10.21037/atm-21-4318). The authors have no conflicts of interest to declare.

Ethical Statement: The authors are accountable for all aspects of the work in ensuring that questions related to the accuracy or integrity of any part of the work are appropriately investigated and resolved. The animal experiments were performed under a project license (No.: 2021-AE026) granted by the Institutional Animal Care Committee of Hebei Medical University, in compliance with AAALAC and the IACUC guidelines for the care and use of animals.

References

1. Ballard C, Gauthier S, Corbett A, et al. Alzheimer's disease. Lancet 2011;377:1019-31.
2. Tiwari S, Atluri V, Kaushik A, et al. Alzheimer's disease: pathogenesis, diagnostics, and therapeutics. Int J Nanomedicine 2019;14:5541-54.
3. Cortes-Canteli M, Iadecola C. Alzheimer's disease and vascular aging: JACC focus seminar. J Am Coll Cardiol 2020;75:942-51.
4. Calvo-Rodriguez M, Kharitonova EK, Bacskai BJ. Therapeutic strategies to target calcium dysregulation in Alzheimer's disease. Cells 2020;9:2513.
5. Alzheimer's Association Calcium Hypothesis Workgroup. Calcium Hypothesis of Alzheimer's disease and brain aging: a framework for integrating new evidence into a comprehensive theory of pathogenesis. Alzheimers Dement 2017;13:178-82.e17.
6. van der Kant R, Langness VF, Herrera CM, et al. Cholesterol metabolism is a druggable axis that independently regulates Tau and amyloid-β in iPSC-derived Alzheimer's disease neurons. Cell Stem Cell 2019;24:363-75.e9.
7. Toledo JB, Arnold M, Kastenmüller G, et al. Metabolic network failures in Alzheimer's disease: A biochemical road map. Alzheimers Dement 2017;13:965-84.
8. Oliver D, Reddy PH. Dynamics of dynamin-related protein 1 in Alzheimer's disease and other neurodegenerative diseases. Cells 2019;8:961.
9. Area-Gomez E, Schon EA. On the pathogenesis of

Alzheimer's disease: the MAM hypothesis. FASEB J 2017;31:864-7.
10. Sun C, Fu Z, Wang S, et al. Roles of tRNA-derived fragments in human cancers. Cancer Lett 2018;414:16-25.
11. Prehn JHM, Jirström E. Angiogenin and tRNA fragments in Parkinson's disease and neurodegeneration. Acta Pharmacol Sin 2020;41:442-6.
12. Idda ML, Munk R, Abdelmohsen K, et al. Noncoding RNAs in Alzheimer's disease. Wiley Interdiscip Rev RNA 2018. doi: 10.1002/wrna.1463.
13. Bahlakeh G, Gorji A, Soltani H, et al. MicroRNA alterations in neuropathologic cognitive disorders with an emphasis on dementia: Lessons from animal models. J Cell Physiol 2021;236:806-23.
14. Anderson P, Ivanov P. tRNA fragments in human health and disease. FEBS Lett 2014;588:4297-304.
15. Kumar P, Anaya J, Mudunuri SB, et al. Meta-analysis of tRNA derived RNA fragments reveals that they are evolutionarily conserved and associate with AGO proteins to recognize specific RNA targets. BMC Biol 2014;12:78.
16. Gagnon KT, Corey DR. Argonaute and the nuclear RNAs: new pathways for RNA-mediated control of gene expression. Nucleic Acid Ther 2012;22:3-16.
17. Yeung ML, Bennasser Y, Watashi K, et al. Pyrosequencing of small non-coding RNAs in HIV-1 infected cells: evidence for the processing of a viral-cellular double-stranded RNA hybrid. Nucleic Acids Res 2009;37:6575-86.
18. Sharma U, Conine CC, Shea JM, et al. Biogenesis and function of tRNA fragments during sperm maturation and fertilization in mammals. Science 2016;351:391-6.
19. Couvillion MT, Bounova G, Purdom E, et al. A Tetrahymena Piwi bound to mature tRNA 3' fragments activates the exonuclease Xrn2 for RNA processing in the nucleus. Mol Cell 2012;48:509-20.
20. Emara MM, Ivanov P, Hickman T, et al. Angiogenin-induced tRNA-derived stress-induced RNAs promote stress-induced stress granule assembly. J Biol Chem 2010;285:10959-68.
21. Goodarzi H, Liu X, Nguyen HC, et al. Endogenous tRNA-derived fragments suppress breast cancer progression via YBX1 displacement. Cell 2015;161:790-802.
22. Huang B, Yang H, Cheng X, et al. tRF/miR-1280 suppresses stem cell-like cells and metastasis in colorectal cancer. Cancer Res 2017;77:3194-206.
23. Deng J, Ptashkin RN, Chen Y, et al. Respiratory syncytial virus utilizes a tRNA fragment to suppress antiviral responses through a novel targeting mechanism. Mol Ther 2015;23:1622-9.
24. Wang Q, Lee I, Ren J, et al. Identification and functional characterization of tRNA-derived RNA fragments (tRFs) in respiratory syncytial virus infection. Mol Ther 2013;21:368-79.
25. Chen Q, Yan M, Cao Z, et al. Sperm tsRNAs contribute to intergenerational inheritance of an acquired metabolic disorder. Science 2016;351:397-400.
26. Short AK, Yeshurun S, Powell R, et al. Exercise alters mouse sperm small noncoding RNAs and induces a transgenerational modification of male offspring conditioned fear and anxiety. Transl Psychiatry 2017;7:e1114.
27. Zhang S, Li H, Zheng L, et al. Identification of functional tRNA-derived fragments in senescence-accelerated mouse prone 8 brain. Aging (Albany NY) 2019;11:10485-98.
28. Wu W, Lee I, Spratt H, et al. tRNA-derived fragments in Alzheimer's disease: implications for new disease biomarkers and neuropathological mechanisms. J Alzheimers Dis 2021;79:793-806.
29. Li S, Xu Z, Sheng J. tRNA-derived small RNA: a novel regulatory small non-coding RNA. Genes (Basel) 2018;9:246.
30. Shen Y, Yu X, Zhu L, et al. Transfer RNA-derived fragments and tRNA halves: biogenesis, biological functions and their roles in diseases. J Mol Med (Berl) 2018;96:1167-76.
31. Li Q, Hu B, Hu GW, et al. tRNA-derived small non-coding RNAs in response to ischemia inhibit angiogenesis. Sci Rep 2016;6:20850.
32. Wang C, Zhao M, Wang J, et al. Expression analysis of transfer RNA-derived fragments in the blood of patients with moyamoya disease: a preliminary study. Mol Med Rep 2019;19:3564-74.
33. Muñoz-Cabrera JM, Sandoval-Hernández AG, Niño A, et al. Bexarotene therapy ameliorates behavioral deficits and induces functional and molecular changes in very-old Triple Transgenic Mice model of Alzheimer´s disease. PLoS One 2019;14:e0223578.
34. Langmead B, Trapnell C, Pop M, et al. Ultrafast and memory-efficient alignment of short DNA sequences to the human genome. Genome Biol 2009;10:R25.
35. Robinson MD, McCarthy DJ, Smyth GK. edgeR: a Bioconductor package for differential expression analysis of digital gene expression data. Bioinformatics 2010;26:139-40.
36. Kim HK, Fuchs G, Wang S, et al. A transfer-RNA-derived small RNA regulates ribosome biogenesis. Nature

2017;552:57-62.
37. Karaiskos S, Naqvi AS, Swanson KE, et al. Age-driven modulation of tRNA-derived fragments in Drosophila and their potential targets. Biol Direct 2015;10:51.
38. Kuscu C, Kumar P, Kiran M, et al. tRNA fragments (tRFs) guide Ago to regulate gene expression post-transcriptionally in a Dicer-independent manner. RNA 2018;24:1093-105.
39. Chan PP, Lowe TM. GtRNAdb: a database of transfer RNA genes detected in genomic sequence. Nucleic Acids Res 2009;37:D93-7.
40. Lowe TM, Chan PP. tRNAscan-SE On-line: integrating search and context for analysis of transfer RNA genes. Nucleic Acids Res 2016;44:W54-7.
41. Wang X, Zheng W. Ca2+ homeostasis dysregulation in Alzheimer's disease: a focus on plasma membrane and cell organelles. FASEB J 2019;33:6697-712.
42. Chen RS, Deng TC, Garcia T, et al. Calcium channel gamma subunits: a functionally diverse protein family. Cell Biochem Biophys 2007;47:178-86.
43. Raffaello A, Mammucari C, Gherardi G, et al. Calcium at the center of cell signaling: interplay between endoplasmic reticulum, mitochondria, and lysosomes. Trends Biochem Sci 2016;41:1035-49.
44. Esquerda-Canals G, Montoliu-Gaya L, Güell-Bosch J, et al. Mouse models of Alzheimer's disease. J Alzheimers Dis 2017;57:1171-83.
45. Mo D, Jiang P, Yang Y, et al. A tRNA fragment, 5'-tiRNAVal, suppresses the Wnt/β-catenin signaling pathway by targeting FZD3 in breast cancer. Cancer Lett 2019;457:60-73.
46. Jia L, Piña-Crespo J, Li Y. Restoring Wnt/β-catenin signaling is a promising therapeutic strategy for Alzheimer's disease. Mol Brain 2019;12:104.
47. Mo D, He F, Zheng J, et al. tRNA-Derived Fragment tRF-17-79MP9PP attenuates cell invasion and migration via THBS1/TGF-β1/Smad3 axis in breast cancer. Front Oncol 2021;11:656078.
48. Le Y, Iribarren P, Gong W, et al. TGF-beta1 disrupts endotoxin signaling in microglial cells through Smad3 and MAPK pathways. J Immunol 2004;173:962-8.
49. Kim EK, Choi EJ. Compromised MAPK signaling in human diseases: an update. Arch Toxicol 2015;89:867-82.
50. Hollnagel JO, Elzoheiry S, Gorgas K, et al. Early alterations in hippocampal perisomatic GABAergic synapses and network oscillations in a mouse model of Alzheimer's disease amyloidosis. PLoS One 2019;14:e0209228.
51. Nevado-Holgado AJ, Ribe E, Thei L, et al. Genetic and real-world clinical data, combined with empirical validation, nominate jak-stat signaling as a target for Alzheimer's disease therapeutic development. Cells 2019;8:425.
52. Tamagnini F, Burattini C, Casoli T, et al. Early impairment of long-term depression in the perirhinal cortex of a mouse model of Alzheimer's disease. Rejuvenation Res 2012;15:231-4.
53. Zhu L, Ge J, Li T, et al. tRNA-derived fragments and tRNA halves: the new players in cancers. Cancer Lett 2019;452:31-7.
54. Sobala A, Hutvagner G. Small RNAs derived from the 5' end of tRNA can inhibit protein translation in human cells. RNA Biol 2013;10:553-63.
55. Gebetsberger J, Zywicki M, Künzi A, et al. tRNA-derived fragments target the ribosome and function as regulatory non-coding RNA in Haloferax volcanii. Archaea 2012;2012:260909.
56. Ivanov P, Emara MM, Villen J, et al. Angiogenin-induced tRNA fragments inhibit translation initiation. Mol Cell 2011;43:613-23.
57. Lyons SM, Achorn C, Kedersha NL, et al. YB-1 regulates tiRNA-induced Stress Granule formation but not translational repression. Nucleic Acids Res 2016;44:6949-60.
58. Elbarbary RA, Takaku H, Uchiumi N, et al. Human cytosolic tRNase ZL can downregulate gene expression through miRNA. FEBS Lett 2009;583:3241-6.
59. Fricker R, Brogli R, Luidalepp H, et al. A tRNA half modulates translation as stress response in Trypanosoma brucei. Nat Commun 2019;10:118.
60. Schampel A, Kuerten S. Danger: high voltage-the role of voltage-gated calcium channels in central nervous system pathology. Cells 2017;6:43.
61. Chakroborty S, Goussakov I, Miller MB, et al. Deviant ryanodine receptor-mediated calcium release resets synaptic homeostasis in presymptomatic 3xTg-AD mice. J Neurosci 2009;29:9458-70.
62. Thibault O, Gant JC, Landfield PW. Expansion of the calcium hypothesis of brain aging and Alzheimer's disease: minding the store. Aging Cell 2007;6:307-17.
63. Schon EA, Area-Gomez E. Mitochondria-associated ER membranes in Alzheimer disease. Mol Cell Neurosci 2013;55:26-36.
64. Jadiya P, Kolmetzky DW, Tomar D, et al. Impaired mitochondrial calcium efflux contributes to disease progression in models of Alzheimer's disease. Nat

Commun 2019;10:3885.
65. Toglia P, Cheung KH, Mak DO, et al. Impaired mitochondrial function due to familial Alzheimer's disease-causing presenilins mutants via Ca(2+) disruptions. Cell Calcium 2016;59:240-50.
66. Arikkath J, Campbell KP. Auxiliary subunits: essential components of the voltage-gated calcium channel complex. Curr Opin Neurobiol 2003;13:298-307.
67. Kang MG, Campbell KP. Gamma subunit of voltage-activated calcium channels. J Biol Chem 2003;278:21315-8.
68. Klugbauer N, Marais E, Hofmann F. Calcium channel alpha2delta subunits: differential expression, function, and drug binding. J Bioenerg Biomembr 2003;35:639-47.
69. Ferron L, Davies A, Page KM, et al. The stargazin-related protein gamma 7 interacts with the mRNA-binding protein heterogeneous nuclear ribonucleoprotein A2 and regulates the stability of specific mRNAs, including CaV2.2. J Neurosci 2008;28:10604-17.
70. Sandoval A, Andrade A, Beedle AM, et al. Inhibition of recombinant N-type Ca(V) channels by the gamma 2 subunit involves unfolded protein response (UPR)-dependent and UPR-independent mechanisms. J Neurosci 2007;27:3317-27.
71. Liu SJ, Gasperini R, Foa L, et al. Amyloid-beta decreases cell-surface AMPA receptors by increasing intracellular calcium and phosphorylation of GluR2. J Alzheimers Dis 2010;21:655-66.
72. Zhang Y, Guo O, Huo Y, et al. Amyloid-β Induces AMPA Receptor Ubiquitination and Degradation in Primary Neurons and Human Brains of Alzheimer's Disease. J Alzheimers Dis 2018;62:1789-801.
73. Milstein AD, Zhou W, Karimzadegan S, et al. TARP subtypes differentially and dose-dependently control synaptic AMPA receptor gating. Neuron 2007;55:905-18.
74. Ghyselinck NB, Duester G. Retinoic acid signaling pathways. Development 2019;146:dev167502.
75. Conaway HH, Henning P, Lerner UH. Vitamin a metabolism, action, and role in skeletal homeostasis. Endocr Rev 2013;34:766-97.
76. Goncalves MB, Clarke E, Hobbs C, et al. Amyloid β inhibits retinoic acid synthesis exacerbating Alzheimer disease pathology which can be attenuated by an retinoic acid receptor α agonist. Eur J Neurosci 2013;37:1182-92.
77. Takasaki J, Ono K, Yoshiike Y, et al. Vitamin A has anti-oligomerization effects on amyloid-β in vitro. J Alzheimers Dis 2011;27:271-80.
78. Ding Y, Qiao A, Wang Z, et al. Retinoic acid attenuates beta-amyloid deposition and rescues memory deficits in an Alzheimer's disease transgenic mouse model. J Neurosci 2008;28:11622-34.
79. Rinaldi P, Polidori MC, Metastasio A, et al. Plasma antioxidants are similarly depleted in mild cognitive impairment and in Alzheimer's disease. Neurobiol Aging 2003;24:915-9.
80. Mullan K, Williams MA, Cardwell CR, et al. Serum concentrations of vitamin E and carotenoids are altered in Alzheimer's disease: a case-control study. Alzheimers Dement (N Y) 2017;3:432-9.
81. Goodman AB, Pardee AB. Evidence for defective retinoid transport and function in late onset Alzheimer's disease. Proc Natl Acad Sci U S A 2003;100:2901-5.

(English Language Editor: J. Jones)

Cite this article as: Lu H, Liu L, Han S, Wang B, Qin J, Bu K, Zhang Y, Li Z, Ma L, Tian J, Zhang K, Li T, Cui H, Liu X. Expression of tiRNA and tRF in *APP/PS1* transgenic mice and the change of related proteins expression. Ann Transl Med 2021;9(18):1457. doi: 10.21037/atm-21-4318

Supplementary

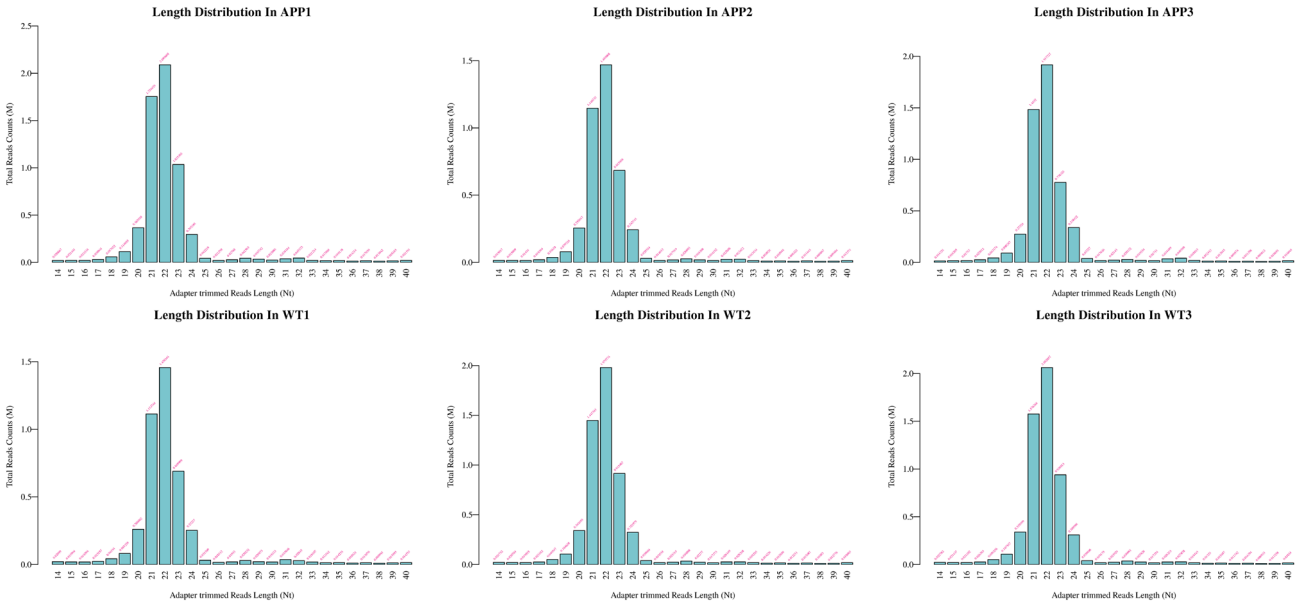

Figure S1 Reads length distribution. Bar chart showing the total read counts against the lengths of the trimmed reads in APP group and WT group. WT, wild type.

https://dx.doi.org/10.21037/atm-21-4318

Table S1 The differentially expressed tiRNA & tRF—up regulated fragments

tRF_ID	Type	APP_CPM	WT_CPM	P value
tRF-Pro-TGG-003	tRF-5b	3.918208221	–0.430741915	0.031078587
tRF-Gly-GCC-025	tRF-3b	5.060777865	3.092198157	0.029301719
tRF-Val-AAC-018	tRF-5c	5.451686522	3.637713762	0.016623329
tRF-His-GTG-021	tRF-5c	6.396095478	4.799040814	0.002931633
tRF-His-GTG-022	tRF-5c	9.484129065	8.265494858	0.002471609
tRF-Val-AAC-011	tRF-5c	7.542456785	6.335793862	0.00953863
tRF-Gly-CCC-042	tRF-3b	7.474973415	6.293579682	0.007227524
tRF-Pro-AGG-012	tRF-5c	7.428967082	6.295278502	0.034281415
tRF-Val-AAC-015	tRF-5b	6.779608645	5.774095772	0.038952452
tRF-Val-AAC-030	tRF-5c	7.366170048	6.412679839	0.038987345
tRF-Thr-CGT-003	tRF-1	11.13168456	10.18116425	0.025793052
tiRNA-Val-CAC-004	tiRNA-5	10.73050923	9.858571219	0.040018543
tRF-Val-CAC-018	tRF-5c	8.667445792	7.816824878	0.040130588
tRF-His-GTG-023	tRF-5c	9.307673567	8.513180181	0.046638123

tRF-ID: the ID of tiRNA & tRF; type: the type of tiRNA & tRF; CPM: the average of log scaled CPM in APP/PS1 group and WT group. WT, wild type; CPM, counts per million.

https://dx.doi.org/10.21037/atm-21-4318

Table S2 The differentially expressed tiRNA & tRF—down regulated fragments

tRF_ID	Type	APP_CPM	WT_CPM	P value
tRF-Gln-CTG-043	tRF-1	–0.430741915	4.33025354	0.012796723
tRF-Val-TAC-031	tRF-5a	–0.430741915	4.163036266	0.012276542
tRF-Cys-GCA-057	tRF-3a	–0.430741915	4.078630202	0.024553934
tRF-Met-CAT-060	tRF-1	1.481813106	4.49786568	0.026757942
tRF-Gly-CCC-012	tRF-5a	2.245551794	4.56990653	0.049710281
tRF-Leu-AAG-005	tRF-5a	5.356161992	7.420782198	0.000118957
tRF-Val-TAC-010	tRF-5c	3.433140488	5.157205194	0.032538791
tRF-Leu-AAG-011	tRF-5a	4.384197918	5.845875259	0.015949521
tRF-Leu-CAA-004	tRF-5a	8.70846735	10.01239671	0.000603854
tRF-Ala-AGC-011	tRF-5a	5.658659869	6.82591079	0.018163377
tRF-Leu-TAG-011	tRF-5a	6.125724078	7.110868555	0.033044413
tRF-Ala-AGC-013	tRF-5a	7.223359012	8.167397183	0.02813504
tRF-Leu-TAG-015	tRF-2	6.444652493	7.306943219	0.047735452

tRF-ID: the ID of tiRNA & tRF; type: the type of tiRNA & tRF; CPM: the average of log scaled CPM in APP/PS1 group and WT group. WT, wild type; CPM, counts per million.

https://dx.doi.org/10.21037/atm-21-4318